Impact of Lorentz forces on Fe3O4-water ferrofluid entropy and exergy treatment within a permeable semi annulus

Sheikholeslami, Mohsen; Arabkoohsar, Ahmad; Khan, Ilyas; Shafee, Ahmad; Li, Zhixiong

Published in:
Journal of Cleaner Production

DOI (link to publication from Publisher):
10.1016/j.jclepro.2019.02.075

Publication date:
2019

Document Version
Accepted author manuscript, peer reviewed version

Accepted Manuscript

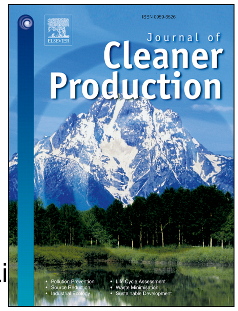

Impact of Lorentz forces on Fe_3O_4-water ferrofluid entropy and exergy treatment within a permeable semi annulus

Mohsen Sheikholeslami, Ahmad Arabkoohsar, Ilyas Khan, Ahmad Shafee, Zhixiong Li

PII: S0959-6526(19)30460-3

DOI: https://doi.org/10.1016/j.jclepro.2019.02.075

Reference: JCLP 15805

To appear in: *Journal of Cleaner Production*

Received Date: 5 September 2018

Revised Date: 4 February 2019

Accepted Date: 7 February 2019

Please cite this article as: Sheikholeslami M, Arabkoohsar A, Khan I, Shafee A, Li Z, Impact of Lorentz forces on Fe_3O_4-water ferrofluid entropy and exergy treatment within a permeable semi annulus, *Journal of Cleaner Production* (2019), doi: https://doi.org/10.1016/j.jclepro.2019.02.075.

Impact of Lorentz forces on Fe_3O_4-water ferrofluid entropy and exergy treatment within a permeable semi annulus

Mohsen Sheikholeslami [a,b], Ahmad Arabkoohsar [c], Ilyas Khan [d,e,1] , Ahmad Shafee [f,g], Zhixiong Li [h,i]

[a] *Department of Mechanical Engineering, Babol Noshirvani University of Technology, Babol, Iran*
[b] *Renewable energy systems and nanofluid applications in heat transfer Laboratory, Babol Noshirvani University of Technology, Babol, Iran*
[c] *Department of Energy Technology, Aalborg University, Denmark*
[d] *Department of Mathematics, College of Science Al-Zulfi, Majmaah University, Al-Majmaah, 11952, Saudi Arabiat*
[e] *Faculty of Mathematics and Statistics, Ton Duc Thang University, Ho Chi Minh City, Vietnam.*

[f] *FAST, University Tun Hussein Onn Malaysia, 86400, Parit Raja, Batu Pahat, Johor State, Malaysia*
[g] *Public Authority of Applied Education and Training, College of Technological Studies, Applied Science Department, Shuwaikh, Kuwait*
[h] *School of Engineering, Ocean University of China, Qingdao 266110, China*
[i] *School of Mechanical, Materials, Mechatronic and Biomedical Engineering, University of Wollongong, Wollongong, NSW 2522, Australia*

Abstract

Challenge of energy will be increase in whole world by augmenting relevance of industry with fossil energy. According to this fact, renewable energies become popular in recent years. Employing nanofluids can help scientists to improve the performance of such systems. The impact of iron oxide–water nanofluid, as working fluid, was employed to evaluate entropy generation in an enclosure in existence of magnetic force. To analyze the performance of heating unit, both view of first and second law of thermodynamic should be involved. In current research, environment-friendly magnetic fluid namely Fe_3O_4-water ferrofluid has been studied which is useful in magnetic nanostructured materials have been found to be very efficient in wastewater decontamination. More exactly, the behavior of magnetic nanofluid through a porous space with innovative computational method is

[1] *Corresponding Author:

Emails: ilyaskhan@tdt.edu.vn (Ilyas Khan); First author: mohsen.sheikholeslami@nit.ac.ir (Mohsen Sheikholeslami)

displayed. To involving porous media, non-Darcy approach was considered. Outcomes are obtained via Control volume based finite element method (CVFEM) to portray the impacts of Hartmann, Rayleigh numbers and permeability. Results display that dispersing nanoparticles leads to augment in thermal performance and decrease in entropy generation. As permeability enhances, Bejan number improves. As Lorentz forces augments, impact of adding nanoparticles reduces and exergy loss detracts. Dispersing nanoparticles are more beneficial in lower values of permeability.

Keywords**:** Nanofluid; Entropy; Porous; Heat transfer; Exergy and CVFEM; Magnetic field.

Nomenclature

S_{gen}	Entropy generation	***Greek symbols***	
X_d	Exergy loss	σ	Electrical conductivity
Nu	Nusselt number	Ω	vorticity
Ha	Hartmann number	θ	temperature
g	gravity	υ	Kinetic viscosity
T	Temperature	β	Thermal expansion coefficient
Be	Bejan number	***Subscripts***	
B	Magnetic field	nf	Nanofluid
Ra	Rayleigh number	M	magnetic
		p	porous

1. Introduction

Nanofluids are the greatest popular tool to augment the efficiency of thermal equipment. Various kinds of nanoparticles have been employed because they can improve conductivity. This kind of working fluids can be used in renewable energy systems for various applications. Bellos et al. (2018) scrutinized different applications of nanofluid in renewable energies. They focus on solar technologies and presented variation of thermal performance in each cases. Nazari et al. (2019) provided solar experimental set up to examine the thermal performance of nanofluid. They utilized cooper oxide nanoparticle for single slope solar still. The productivity of fresh water augments with adding nanoparticles. Nan et al. (2019) scrutinized clean way for producing magnetic nanoparticles. Sheikholeslami et al. (2019a) utilized nanoparticles for solar heat storage unit. They suggested new shapes for metallic fin. Hayat et al. (2017) scrutinized nanofluid concentration analysis in a three dimensional enclosure. Entropy generation of nanoparticles within a porous space was demonstrated by Sheikholeslami (2019a). He considered magnetic force influence on exergy loss. Qi et al. (2017) scrutinized the silver nanoparticle migration in a cavity by using numerical method. Working fluid can be considered as non-Newtonian fluid when nanoparticles have been added (Khan et al. (2017), Hashim et al. (2018), Abro and Khan (2017)).

Sharafeldin and Gróf (2018) presented an application of CeO2/water nanofluid. They indicated that the outlet temperature augments when nanofluids are utilized. Sheikholeslami et al. (2018a) employed two temperature approaches for porous medium to discover ferrofluid behavior due to magnetic. Utilizing magnetic and electric fields are common ways for controlling flow direction (Mishra et al. (2015), Sheikholeslami and Mahian (2019), Sheikholeslami et al. (2018b,c), Moatimid and Hassan (2018), Muhammad et al. (2018)). Said et al. (2016) carried out the exergy performances of solar collector in existence of alumina nanoparticles. They showed the impact of nanoparticles' size on thermal performance. If domain is porous space, several models can be used for simulation (Zin et al. (2017), Sheikholeslami et al. (2019b), Soomro et al. (2019), Sheikholeslami (2019b)). Ali et al. (2017) employed the fractional model for analyzing nanofluid flow due to magnetic force. They utilized polar coordinate for circular tube. The pollution of water these days has become one of a critical issue throughout the world. However, several water treatment technologies are in continuous efforts for improvement. Amongst them nanomaterials are regarded as an efficient strategy for water decontamination, and for environment protection. However, it is of central focus that the water treatment methodologies themselves should not produce additional harmful materials but should use instead non-toxic biodegradable ones. In this work, ferrofluid have been involved which is indeed a potential candidate for water remediation and for the homogenous dispersion of magnetite nanoparticles (NPs) in aqueous solution. Recent years, to enhance the thermal performance, nanoparticles and other passive ways have been utilized (Sheikholeslami (2018), Lee et al. (2018), Sheikholeslami et al. (2019c), Qi et al. (2011), Fengrui et al. (2018)).

There is few papers in which, nanofluid exergy and entropy analysis have been done. To reach best design of renewable energy unit, minimizing entropy generation is vital factor. In current text, as an application of magnetic nanoparticles, entropy and exergy analysis of ferrofluid due to magnetic forces within a permeable medium was scrutinized. Powerful numerical method was employed to display the energy and exergy analysis for different values of permeability, Lorentz and buoyancy forces.

2. Geometry explanation

Boundary condition sample element and geometry of current paper has been provided in Fig. 1. Permeable space is full of ferrofluid. Constant heat flux was employed on inner cylinder. Horizontal magnetic field was employed. Both energy and exergy views have been included to reach the best design. Selecting nanofluid causes to improve thermal treatment of system.

3. Formulation and CVFEM

3.1. Governing

The aim of article is to simulate ferrofluid convective flow inside a two dimensional (2D) permeable space with magnetic force. Gravity force is included as buoyancy forces. Non-Darcy model for porous space has been selected. Moreover, for estimating ferrofluid properties, homogeneous model has been assumed. Related formulations are:

$$\frac{\partial v}{\partial y}+\frac{\partial u}{\partial x}=0 \tag{1}$$

$$\rho_{nf}\left(\frac{\partial u}{\partial y}v+u\frac{\partial u}{\partial x}\right)=\left[\sigma_{nf}B_xB_yv-\frac{\mu_{nf}}{K}u-\sigma_{nf}B_y^2u-\frac{\partial P}{\partial x}+\left(\frac{\partial^2 u}{\partial y^2}+\frac{\partial^2 u}{\partial x^2}\right)\mu_{nf}\right], \tag{2}$$
$$\left(B_y,B_x\right)=B_o\left(\sin\gamma,\cos\gamma\right)$$

$$\rho_{nf}\left(v\frac{\partial v}{\partial y}+\frac{\partial v}{\partial x}u\right)=\mu_{nf}\left(\frac{\partial^2 v}{\partial y^2}+\frac{\partial^2 v}{\partial x^2}\right)+g\left(T-T_c\right)\rho_{nf}\beta_{nf} \tag{3}$$
$$-B_xvB_x\sigma_{nf}-\frac{\mu_{nf}}{K}v+B_xu\sigma_{nf}B_y-\frac{\partial P}{\partial y},$$
$$\left(B_y,B_x\right)=B_o\left(\sin\gamma,\cos\gamma\right)$$

$$k_{nf}\left(\frac{\partial^2 T}{\partial x^2}+\frac{\partial^2 T}{\partial y^2}\right)=\left(\rho C_p\right)_{nf}\left(u\frac{\partial T}{\partial x}+\frac{\partial T}{\partial y}v\right) \tag{4}$$

$\left(\rho C_p\right)_{nf}$, $(\rho\beta)_{nf}$, ρ_{nf}, k_{nf} and σ_{nf} are predicted as:

$$\left(\rho C_p\right)_{nf}=\left(\rho C_p\right)_f(1-\phi)+\left(\rho C_p\right)_s\phi \tag{5}$$

$$(\rho\beta)_{nf}=\phi(\rho\beta)_s+(1-\phi)(\rho\beta)_f \tag{6}$$

$$\rho_{nf}=(1-\phi)\rho_f+\rho_s\phi \tag{7}$$

$$k_{nf}=k_f\left(\frac{2k_f+k_s+2\phi(k_s-k_f)}{-(k_s-k_f)\phi+k_s+2k_f}\right) \tag{8}$$

$$\frac{\sigma_{nf}}{\sigma_f}=1+\frac{3(-1+\Delta)\phi}{(2+\Delta)-(-1+\Delta)\phi}\quad ,\sigma_s/\sigma_f=\Delta \tag{9}$$

μ_{nf} is estimated as (Wang et al. (2016)):

$$\mu_{nf}=\left(3.1B-27886.4807\phi^2+0.035B^2+4263.02\phi+316.0629\right)e^{-0.01T}. \tag{10}$$

Properties of ferrofluid have been listed in Table 1. To eliminate pressure terms, below definitions should be involved:

$$\frac{\partial\psi}{\partial y}=u,\quad \frac{\partial u}{\partial y}-\frac{\partial v}{\partial x}=-\omega,\quad v=-\frac{\partial\psi}{\partial x}, \tag{11}$$

Defining non-dimensional quantities:

$$\Theta=\frac{T-T_c}{\Delta T},U=\frac{uL}{\alpha_f},\Delta T=q''L/k_f,V=\frac{vL}{\alpha_f},(X,Y)=\frac{(x,y)}{L} \tag{12}$$

So, following equations can be derived:

$$V\frac{\partial\Theta}{\partial Y}+U\frac{\partial\Theta}{\partial X}=\frac{\partial^2\Theta}{\partial Y^2}+\frac{\partial^2\Theta}{\partial X^2} \tag{13}$$

$$\frac{\partial^2\Psi}{\partial X^2}+\frac{\partial^2\Psi}{\partial Y^2}=-\Omega \tag{14}$$

$$\begin{aligned}&\Pr\left(\frac{A_5A_2}{A_1A_4}\right)\left(\frac{\partial^2\Omega}{\partial Y^2}+\frac{\partial^2\Omega}{\partial X^2}\right)+Ra\Pr\left(\frac{\partial\Theta}{\partial X}\right)\left(\frac{A_3A_2^2}{A_1A_4^2}\right)\\&+Ha^2\Pr\left[\frac{A_6A_2}{A_1A_4}\right]\left(-(\sin\gamma)(\cos\gamma)\frac{\partial V}{\partial Y}+(\cos\gamma)\frac{\partial U}{\partial X}(\sin\gamma)-\frac{\partial V}{\partial X}(\cos\gamma)^2+(\sin\gamma)^2\frac{\partial U}{\partial Y}\right)\\&-\frac{\Pr}{Da}\left(\frac{A_5A_2}{A_1A_4}\right)\Omega=U\frac{\partial\Omega}{\partial X}+\frac{\partial\Omega}{\partial Y}V\end{aligned} \tag{15}$$

Following definitions should be mentioned for dimensionless variables:

$$\begin{aligned}&Da=\frac{K}{L^2},Ra=g\beta_f q''L^4/(k_f\upsilon_f\alpha_f),\\&A_2=\frac{(\rho C_P)_{nf}}{(\rho C_P)_f},Ha=LB_0\sqrt{\sigma_f/\mu_f},\\&A_1=\frac{\rho_{nf}}{\rho_f},\quad A_6=\frac{\sigma_{nf}}{\sigma_f},\ A_5=\frac{\mu_{nf}}{\mu_f},\\&\Pr=\upsilon_f/\alpha_f,A_4=\frac{k_{nf}}{k_f},\ A_3=\frac{(\rho\beta)_{nf}}{(\rho\beta)_f}\end{aligned} \tag{16}$$

and current boundary conditions can be presented as:

$$\Theta=0.0 \qquad \text{@ cold surface} \tag{17}$$

$$\Psi=0.0 \qquad \text{@ all walls}$$

$$\frac{\partial\Theta}{\partial n}=1.0 \qquad \text{@ hot surface}$$

Nu_{loc}, Nu_{ave} and En are determined from:

$$Nu_{loc}=\frac{1}{\theta}\left(\frac{k_{nf}}{k_f}\right) \tag{18}$$

$$Nu_{ave} = \frac{1}{S}\int_0^s Nu_{loc}\, ds \tag{19}$$

$$En = \frac{Nu_{ave}\big|_{\phi=0.04} - Nu_{ave}\big|_{\phi=0}}{Nu_{ave}\big|_{\phi=0}} \times 100$$

Definitions of entropy generation, exergy loss and Bejan number are (Sheikholeslami et al. (2019c)):

$$\begin{aligned} S_{gen,total} = & \underbrace{\frac{\mu_{nf}}{T^2}\left[\left(\frac{\partial u}{\partial y}+\frac{\partial v}{\partial x}\right)^2 + 2\left(\left(\frac{\partial u}{\partial x}\right)^2+\left(\frac{\partial v}{\partial y}\right)^2\right)\right]}_{S_{gen,f}} \\ & + \underbrace{\frac{\sigma_{nf}}{T^2}B_0^2 v^2}_{S_{gen,M}} + \underbrace{\frac{\mu_{nf}}{KT}\left(u^2+v^2\right)}_{S_{gen,P}} \\ & + \underbrace{\frac{k_{nf}}{T^2}\left[\left(\frac{\partial T}{\partial y}\right)^2+\left(\frac{\partial T}{\partial x}\right)^2\right]}_{S_{gen,th}} \end{aligned} \tag{20}$$

$$X_d = T_0 S_{gen,total} \tag{21}$$

$$Be = S_{gen,th} / S_{gen,total} \tag{22}$$

3.2. CVFEM

Innovative method has been applied in current article. The first code of this method was written by Sheikholeslami (2019c). He employed the mention method for various heat transfer problems. Finite element method (FEM) has been merged with Finite volume method (FVM) to generate this new algorithm. Researchers can find more details of this approach in new reference book (Sheikholeslami (2019c)). Current approach uses triangular element for 2D problems (see Fig. 1(b)).

4. Mesh independency and verification

To obtain unique results, various mesh sizes should be tested. One instance exists in table2. Also, Fig. 2 and table3 prove the accuracy of this code. Both nanofluid flow and magnetohydrodynamic (MHD) flow have been checked (Rudraiah et al. (1995), Calcagni et al. (2003), Khanafer et al. (2005)).

5. Results and discussion

Iron oxide-water ferrofluid free convection inside a permeable space was scrutinized in current text. To estimate the viscosity, Lorentz forces effect has been involved. Not only energy analysis but also exergy and entropy treatment have been reported. CVFEM has been employed to depict the results for various Darcy number ($Da = 0.01$ to 100), Magnetic field ($Ha = 1$ to 40) and Rayleigh number ($Ra = 10^3$ to 10^4).

Figs. 3, 4, 5 and 6 are presented to display the influences of *Ra*, *Da* and *Ha* on energy, entropy and exergy behavior of ferrofluid. According to definition of Ra and Da, augmenting such variables lead greater heat transfer. Graphs indicate this fact and it can be seen that convection enhances with rise of buoyancy and permeability. Furthermore, Lorentz forces make the conduction to augment and dispersing nanoparticles have more benefit. Surface temperature reduces with augment of permeability but it improves with augment of magnetic force. $|\psi_{max}|$ augments with augment of *Da* and *Ra* while it declines with rise of *Ha*. Temperature along the inner surface reduces with decrease of magnetic force. Magnetic entropy generation declines with reduce of *Ra* and *Ha*. As Lorentz forces augments, Bejan number augments.

Figs. 7, 8 and 9 illustrate the changes of Be, Nu_{ave}, X_d with variation of *Ra*, *Ha*, and *Da*. Eqs. (23-25) has been derived from simulation data:

$$\begin{aligned} Nu_{ave} &= 0.067 Da\log(Ra) - 0.068\log(Ra)Ha - 0.044 Ha\,Da \\ &+1.82 + 0.17\log(Ra) + 0.081Da - 0.08Ha \end{aligned} \tag{23}$$

$$\begin{aligned} Be &= 0.97 - 8.84\times10^{-3}Da - 0.028\log(Ra) + 8.87\times10^{-3}Ha \\ &-8.5\times10^{-3}Da\log(Ra) + 4.17\times10^{-3}Da\,Ha + 8.5\times10^{-3}\log(Ra)Ha \end{aligned} \tag{24}$$

$$\begin{aligned} X_d &= 105.29 - 2.94Da - 5.31\log(Ra) + 2.86Ha \\ &-2.2Da\log(Ra) + 1.61Da\,Ha + 2.19\log(Ra)Ha \end{aligned} \tag{25}$$

Convective mode has been boosted with rise of *Da* and *Ra*. Also, augmenting magnetic force causes Nu_{ave} to detract. Exergy loss and Bejan number have reverse treatment in comparison with Nu_{ave}. Exergy loss detracts with augment of permeability. Bejan number improves with increase of *Ha*. Fig. 10 displays the variation of heat transfer augmentation (*En*) due to changing Ra, Ha and Da. Dispersing nanoparticles has greater impact in cases with greater conduction. Thus, this factor augments with increase of *Ha* and it decreases with augment of Da and Ra.

6. Conclusions

Magnetic force role on treatment of Ferrofluid flow and entropy generation through a permeable space was reported by employing CVFEM. In current research, environment-friendly magnetic fluid namely Fe_3O_4-water ferrofluid has been studied which is useful in magnetic nanostructured materials have been found to be very efficient in wastewater decontamination. The impact of iron oxide–water nanofluid, as working fluid, was employed to evaluate entropy generation in an enclosure in existence of magnetic force. Different parts of entropy generation are reported as separate contours. Variation of Bejan number and exergy loss are depicted due to changing *Da, Ha* and *Ra*. Bejan number reduces with rise of conduction mode. As these variables augments, magnetic entropy generation enhances. As magnetic forces enhance, exergy loss augments.

Acknowledgements: This paper was supported by the National Sciences Foundation of China (NSFC) (No. U1610109), UOW Vice-Chancellor's Postdoctoral Research Fellowship. Besides, the authors acknowledge the funding support of Babol Noshirvani University of Technology through Grant program No. BNUT/390051/98

References

Abro, K.A., Khan, I., 2017. Analysis of the heat and mass transfer in the MHD flow of a generalized Casson fluid in a porous space via non-integer order derivatives without a singular kernel. Chin. J. Phys. 55, 1583-1595

Ali, F., Sheikh, N.A., Khan, I, Saqib, M., 2017. Magnetic field effect on blood flow of Casson fluid in axisymmetric cylindrical tube: A fractional model. J. Magn. Magn. Mater. 423, 327-336.

Bellos, E., Said, Z., Tzivanidis, C. 2018. The use of nanofluids in solar concentrating technologies: A comprehensive review. J. Clean. Prod. 196, 84-99

Calcagni, B.,, Marsili, F., Paroncini, M., 2005. Natural convective heat transfer in square enclosures heated from below. Appl. Therm. Eng. 25, 2522–2531.

Fengrui, S., Yuedong, Y., Xiangfang, L., 2018. The Heat and Mass Transfer Characteristics of Superheated Steam Coupled with Non-condensing Gases in Horizontal Wells with Multi-point Injection Technique. Energy, 143, 995-1005

Hayat, T., Aziz, A., Muhammad, T., Alsaedi, A., 2017. Three-dimensional flow of nanofluid with heat and mass flux boundary conditions. Chin. J. Phys. 55, 1495-1510.

Hashim, M. Khan, A.S. Alshomrani, Haq, R.U., 2018. Investigation of dual solutions in flow of a non-Newtonian fluid with homogeneous-heterogeneous reactions: Critical points. European J. Mech.-B/Fluids, 68, 30 – 38

Khan, N.S., Gul, T., Islam, S., Kha, A., Shah, Z., 2017. Brownian Motion and Thermophoresis Effects on MHD Mixed Convective Thin Film Second-Grade Nanofluid Flow with Hall Effect and Heat Transfer Past a Stretching Sheet. Journal of Nanofluids 6, 1–18

Khanafer, K., Vafai, K., Lightstone, M., 2003. Buoyancy-driven heat transfer enhancement in a two-dimensional enclosure utilizing nanofluids, Int. J. Heat Mass Transfer 46, 3639–3653

Lee, P., Kim, J.K., Lee, S.W., 2018. Experimental characterization on eco-friendly micro-grinding process of titanium alloy using air flow assisted electrospray lubrication with nanofluid. J. Clean. Prod. 201, 452-462

Muhammad, S., Ali, G., Shah, Z., Islam, S., Hussain, A., 2018. The Rotating Flow of Magneto Hydrodynamic Carbon Nanotubes over a Stretching Sheet with the Impact of Non-Linear Thermal Radiation and Heat Generation/Absorption, Appl. Sci., 8, 0; doi: 10.3390/app8040000).

Mishra, S.R., Pattnaik, P.K., Dash, G.C., 2015. Effect of heat source and double stratification on MHD free convection in a micropolar fluid. Alexandria Eng. J. 54, 681-689

Moatimid G.M., Hassan, M.A., 2018. Linear Instability of Water–Oil Electrohydrodynamic Nanofluid Layers: Analytical and Numerical Study. J. Comput. Theor. Nanos. 15(5), 1495-1510

Nazari, S., Safarzadeh, H., Bahiraei, M., 2019. Performance improvement of a single slope solar still by employing thermoelectric cooling channel and copper oxide nanofluid: An experimental study. J. Clean. Prod.208, 1041-1052

Nan, A., Filip, X., Dan, M., Marincaş, O., 2019. Clean production of new functional coatings of magnetic nanoparticles from sustainable resources. J. Clean. Prod. 210, 687-696

Qi, C., He, Y., Hu, Y., Yang, J., Li, F., Ding, Y., 2011. Natural convection of Cu-Gallium nanofluid in enclosures. ASME J. Heat Transf. 133(12), 122504

Qi, C., Yang, L., Wang, G., 2017. Numerical study on convective heat transfer enhancement in horizontal rectangle enclosures filled with Ag-Ga nanofluid, Nanoscale Res. Lett. 12(1), 326-335

Rudraiah, N., Barron, R.M., Venkatachalappa, M., Subbaraya CK, 1995. Effect of a magnetic field on free convection in a rectangular enclosure, Int. J. Engrg. Sci. 33, 1075–1084.

Sheikholeslami, M., Haq, R.U., Shafee, A., Li, Z., 2019a. Heat transfer behavior of Nanoparticle enhanced PCM solidification through an enclosure with V shaped fins. Int. J. Heat Mass Tran. 130, 1322–1342

Sheikholeslami, M., 2019a. New computational approach for exergy and entropy analysis of nanofluid under the impact of Lorentz force through a porous media, Comput. Method Appl. M. 344, 319–333

Sharafeldin, M.A., Gróf, G., 2018. Evacuated tube solar collector performance using CeO2/water nanofluid. J. Clean. Prod. 185, 347-356

Sheikholeslami, M., Khan, I., Tlili, I., 2018a. Non-equilibrium model for nanofluid free convection inside a porous cavity considering Lorentz forces. Sci. Rep. 8:16881, DOI:10.1038/s41598-018-33079-6

Said, Z., Saidur, R., Rahim, N.A., 2016. Energy and exergy analysis of a flat plate solar collector using different sizes of aluminium oxide based nanofluid. J. Clean. Prod. 133, 518-530

Sheikholeslami, M., Barzegar Gerdroodbary, M., Moradi, R., Shafee, A., Li, Z., 2019b. Application of Neural Network for estimation of heat transfer treatment of Al2O3- H2O nanofluid through a channel. Comput. Method Appl. M. 344, 1–12

Sheikholeslami, M., Jafaryar, M., Shafee, A., Li, Z., 2018b, Investigation of second law and hydrothermal behavior of nanofluid through a tube using passive methods. J. Mol. Liq. 269, 407–416

Sheikholeslami, M., Li, Z., Shafee, A., 2018c. Lorentz forces effect on NEPCM heat transfer during solidification in a porous energy storage system. Int. J. Heat Mass Tran. 127, 665–674

Sheikholeslami, M., 2019b. Numerical approach for MHD Al2O3-water nanofluid transportation inside a permeable medium using innovative computer method. Comput. Method Appl. M. 344, 306–318

Sheikholeslami, M., Mahian, O., 2019. Enhancement of PCM solidification using inorganic nanoparticles and an external magnetic field with application in energy storage systems. J. Clean. Prod.215, 963-977

Sheikholeslami, M., 2019c. Application of Control Volume based Finite Element Method (CVFEM) for Nanofluid Flow and Heat Transfer, Elsevier, ISBN: 9780128141526

Sheikholeslami, M., Jafaryar, M., Shafee, A., Li, Z., 2019c. Nanofluid heat transfer and entropy generation through a heat exchanger considering a new turbulator and CuO nanoparticles. J. Therm. Anal. Calorim. DOI: 10.1007/s10973-018-7866-7

Soomro, F.A., Zaib, A., Haq, R.U., Sheikholeslami, M., 2019. Dual nature solution of water functionalized copper nanoparticles along a permeable shrinking cylinder: FDM approach. Int. J. Heat Mass Tran.129, 1242–1249

Sheikholeslami, M., 2018, Finite element method for PCM solidification in existence of CuO nanoparticles. J. Mol. Liq. 265, 347–355

Wang, L., Wang, Y., Yan, X., Wang, X., Feng, B., 2016. Investigation on viscosity of Fe3O4 nanofluid under magnetic field. Int. Commun. Heat Mass. 72, 23–28

Zin, N.A.M., Khan, I., Shafie, S., Alshomrani, A.S., 2017. Analysis of heat transfer for unsteady MHD free convection flow of rotating Jeffrey nanofluid saturated in a porous medium. Results in Phys., 7 () 288-309

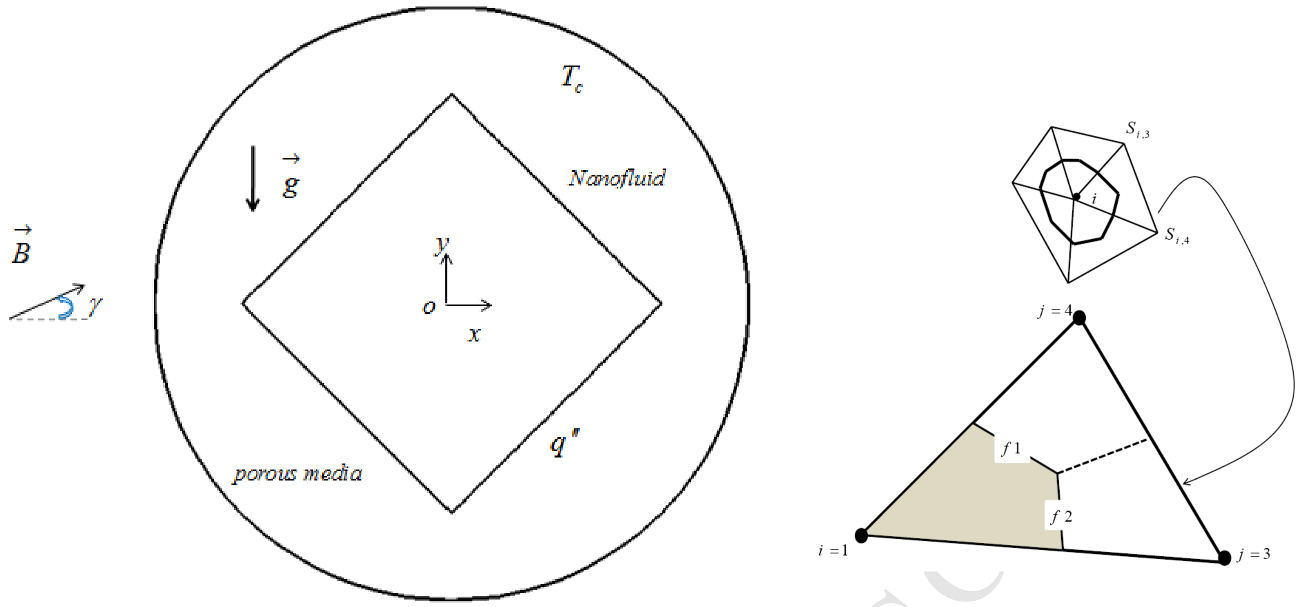

Fig. 1. Porous enclosure under the effect of magnetic field

Present work   Calcagni et al. (2003)

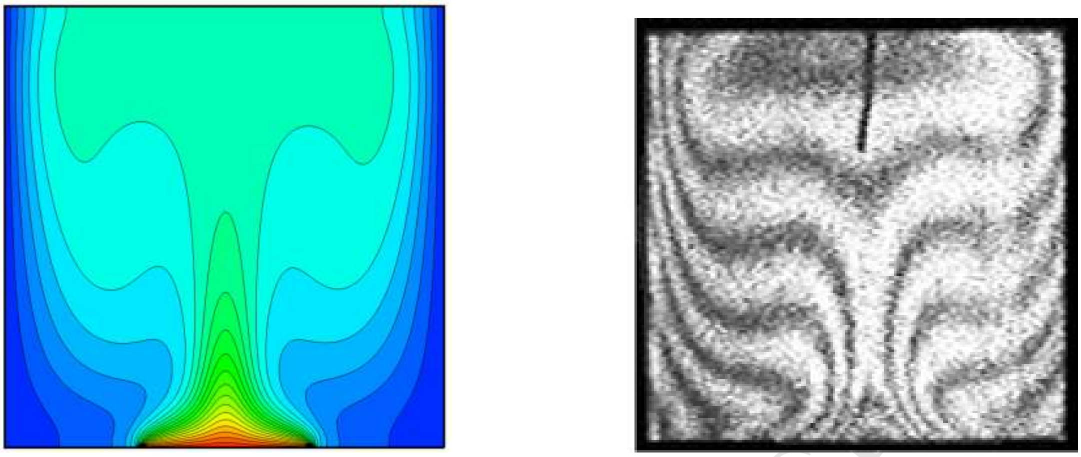

(a)

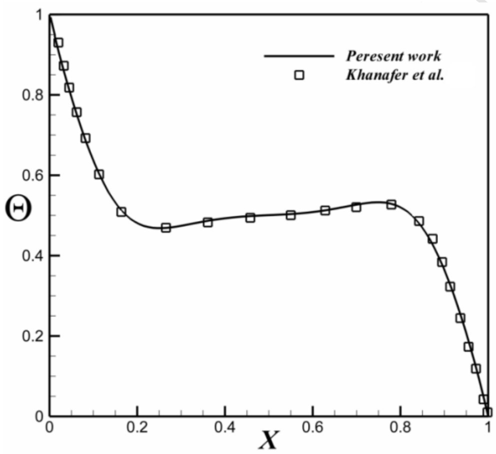

(b) Gr=10^4,

Fig. 2. Validation for (a) natural convection (Calcagni et al. (2003)); (b) nanofluid flow (Khanafer et al. (2005))

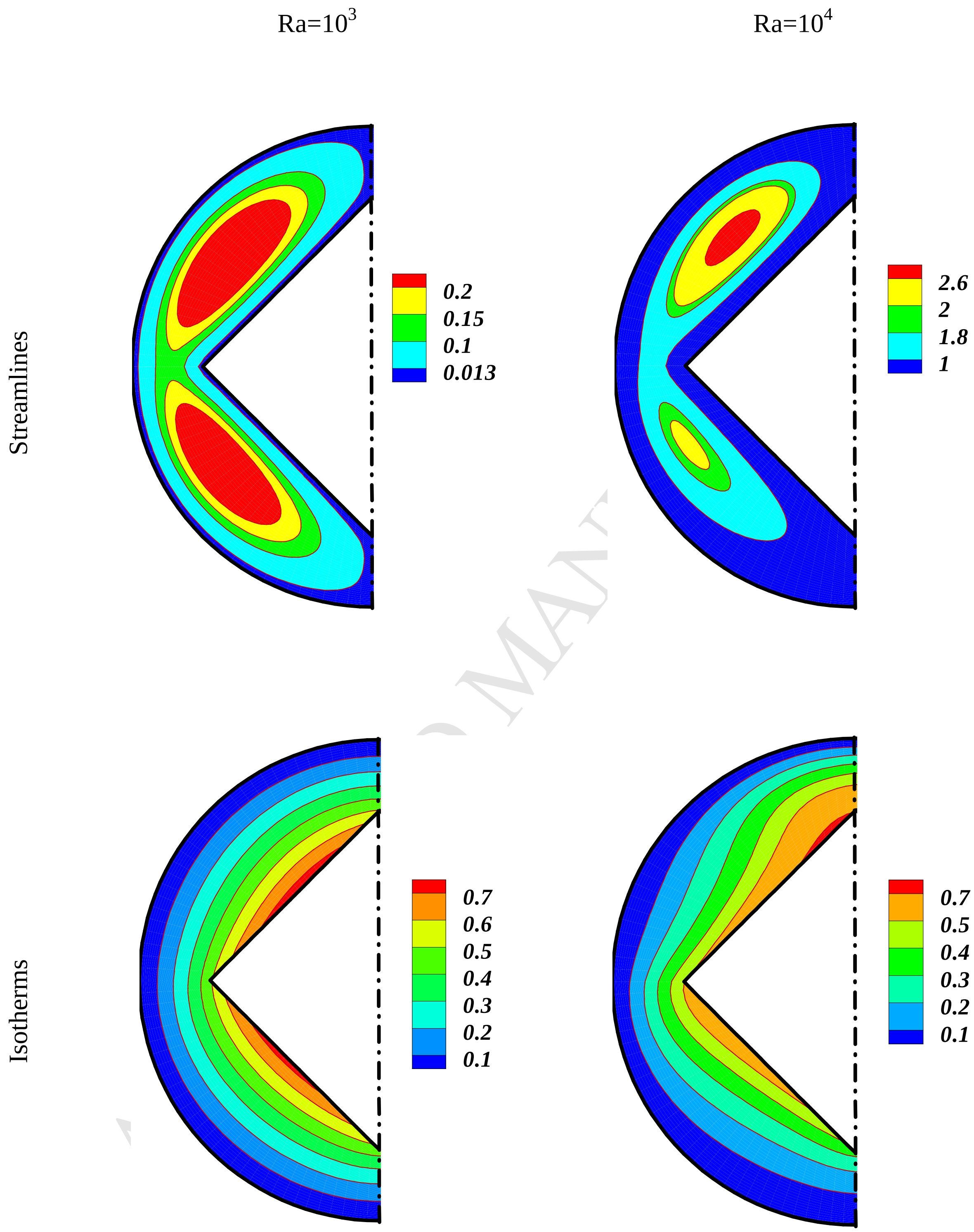

Ra=10^3
Ra=10^4
Streamlines
Isotherms
0.2
0.15
0.1
0.013
2.6
2
1.8
1
0.7
0.6
0.5
0.4
0.3
0.2
0.1
0.7
0.5
0.4
0.3
0.2
0.1

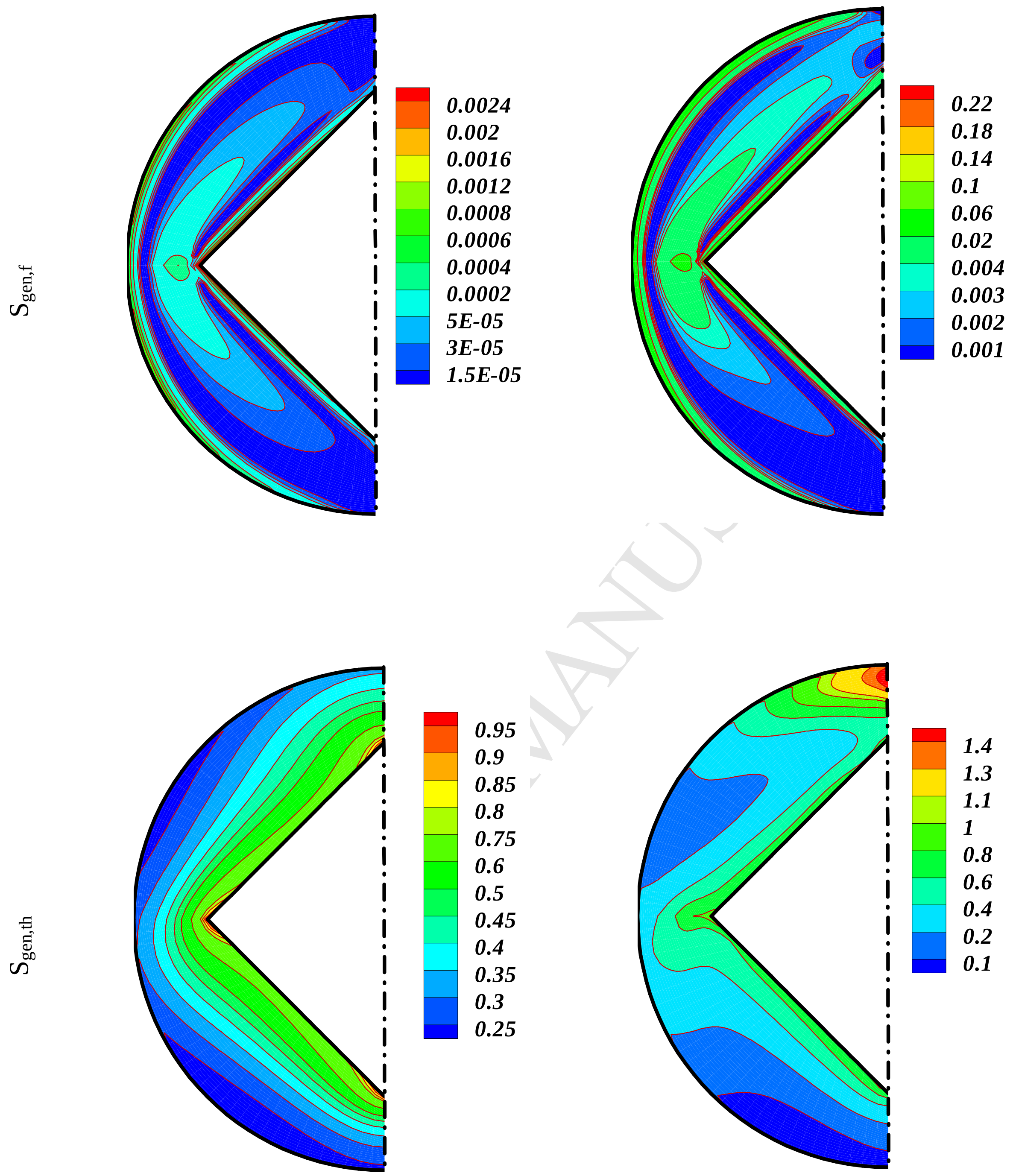

$S_{gen,f}$
0.0024
0.002
0.0016
0.0012
0.0008
0.0006
0.0004
0.0002
5E-05
3E-05
1.5E-05
0.22
0.18
0.14
0.1
0.06
0.02
0.004
0.003
0.002
0.001
$S_{gen,th}$
0.95
0.9
0.85
0.8
0.75
0.6
0.5
0.45
0.4
0.35
0.3
0.25
1.4
1.3
1.1
1
0.8
0.6
0.4
0.2
0.1

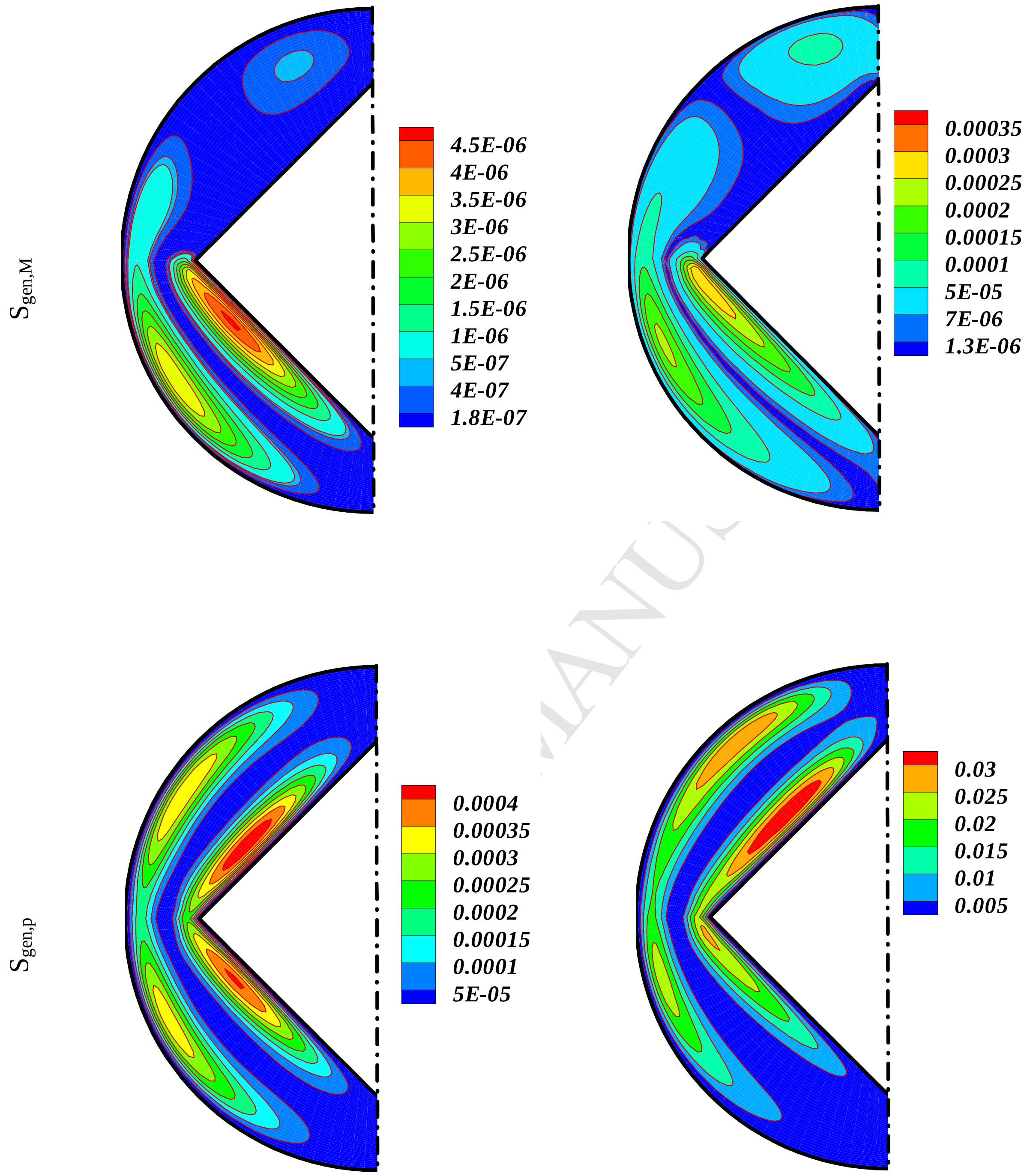

$S_{gen,M}$
4.5E-06
4E-06
3.5E-06
3E-06
2.5E-06
2E-06
1.5E-06
1E-06
5E-07
4E-07
1.8E-07
0.00035
0.0003
0.00025
0.0002
0.00015
0.0001
5E-05
7E-06
1.3E-06
$S_{gen,p}$
0.0004
0.00035
0.0003
0.00025
0.0002
0.00015
0.0001
5E-05
0.03
0.025
0.02
0.015
0.01
0.005

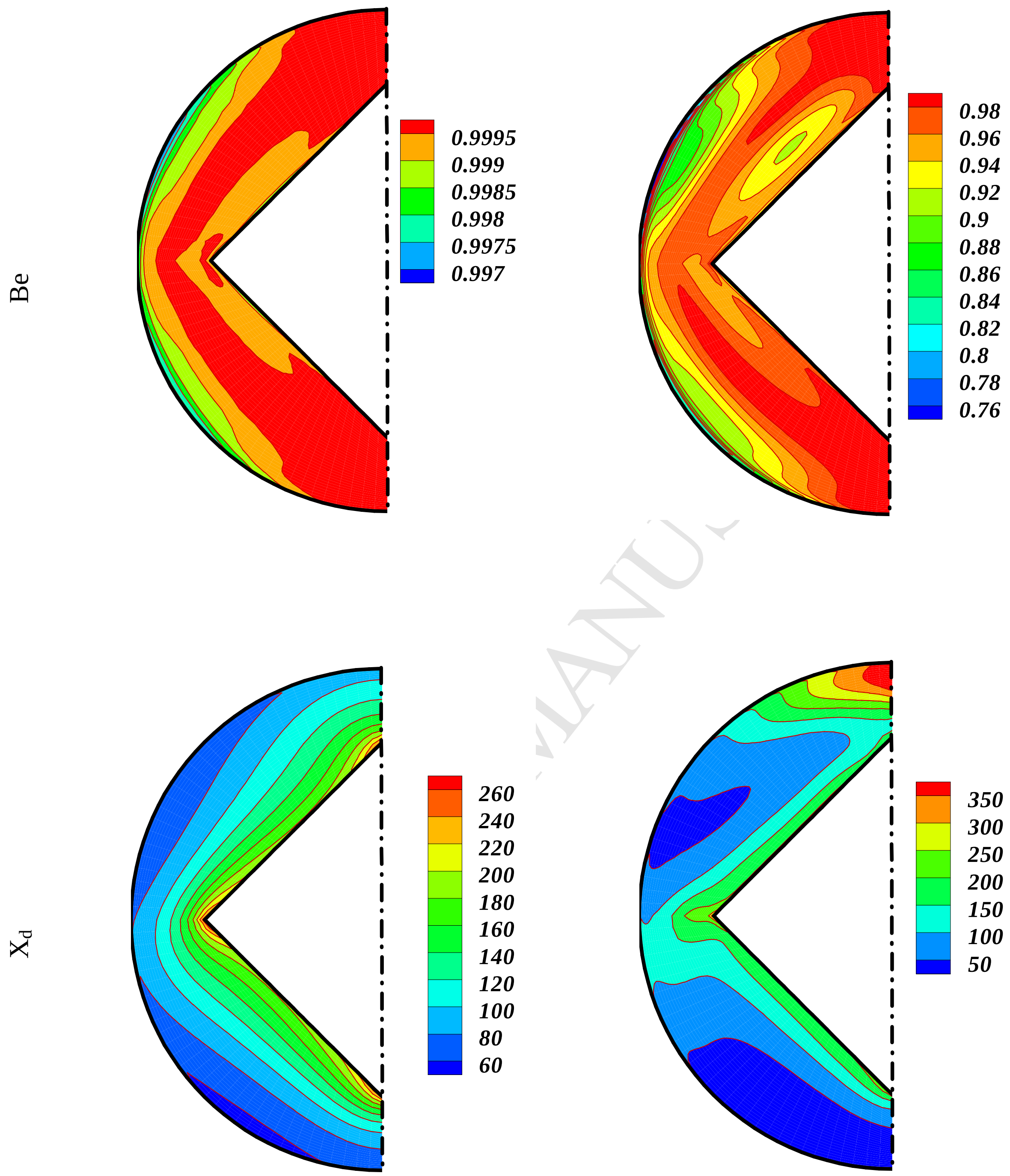

Fig. 3. Exergy and entropy contours for various *Ra* at $\phi = 0.04, Ha = 1, Da = 0.01$

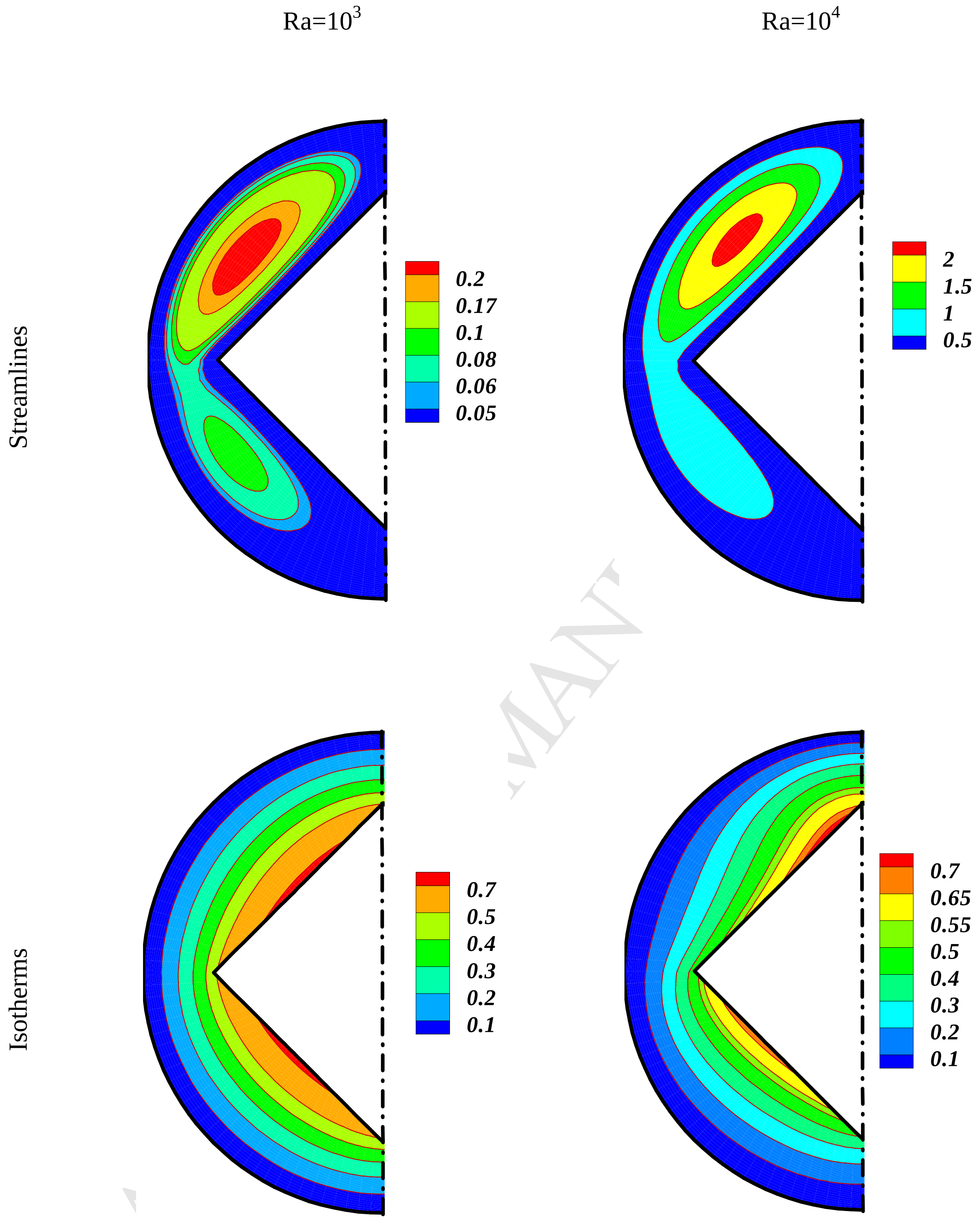
Ra=10^3
Ra=10^4
Streamlines
Isotherms
0.2
0.17
0.1
0.08
0.06
0.05
2
1.5
1
0.5
0.7
0.5
0.4
0.3
0.2
0.1
0.7
0.65
0.55
0.5
0.4
0.3
0.2
0.1

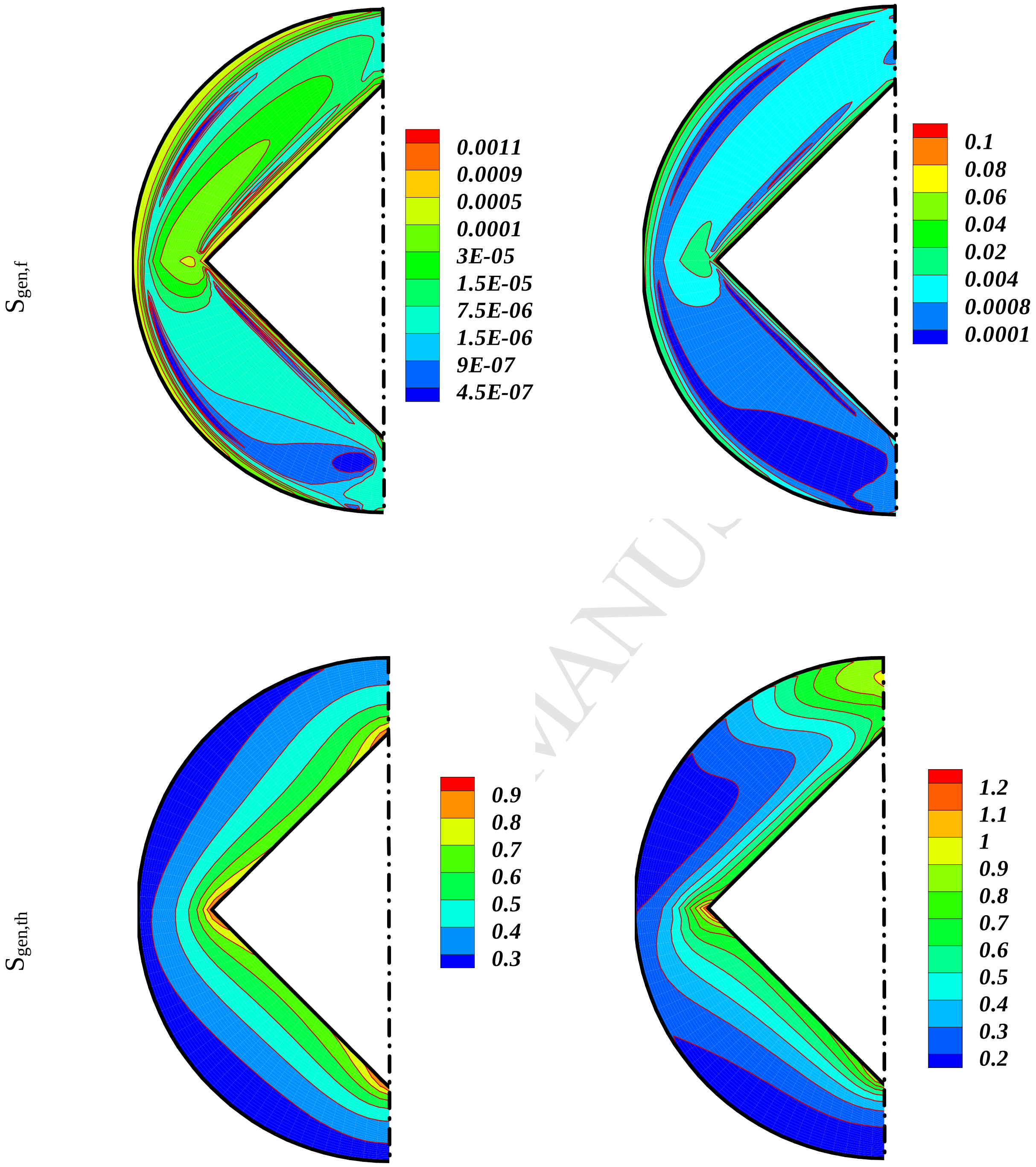
$S_{gen,f}$
0.0011
0.0009
0.0005
0.0001
3E-05
1.5E-05
7.5E-06
1.5E-06
9E-07
4.5E-07
0.1
0.08
0.06
0.04
0.02
0.004
0.0008
0.0001
$S_{gen,th}$
0.9
0.8
0.7
0.6
0.5
0.4
0.3
1.2
1.1
1
0.9
0.8
0.7
0.6
0.5
0.4
0.3
0.2

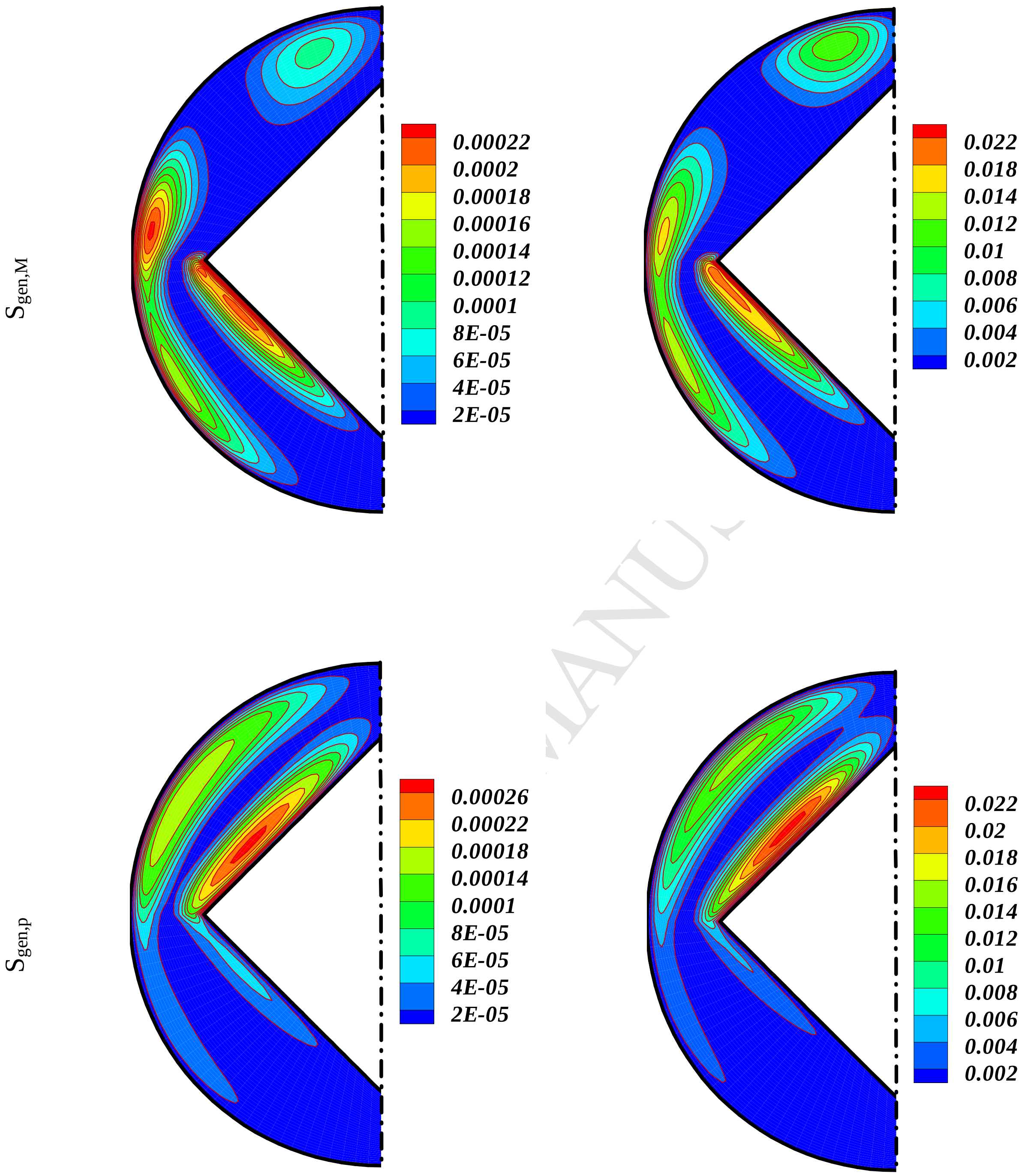

$S_{gen,M}$
0.00022
0.0002
0.00018
0.00016
0.00014
0.00012
0.0001
8E-05
6E-05
4E-05
2E-05
0.022
0.018
0.014
0.012
0.01
0.008
0.006
0.004
0.002
$S_{gen,p}$
0.00026
0.00022
0.00018
0.00014
0.0001
8E-05
6E-05
4E-05
2E-05
0.022
0.02
0.018
0.016
0.014
0.012
0.01
0.008
0.006
0.004
0.002

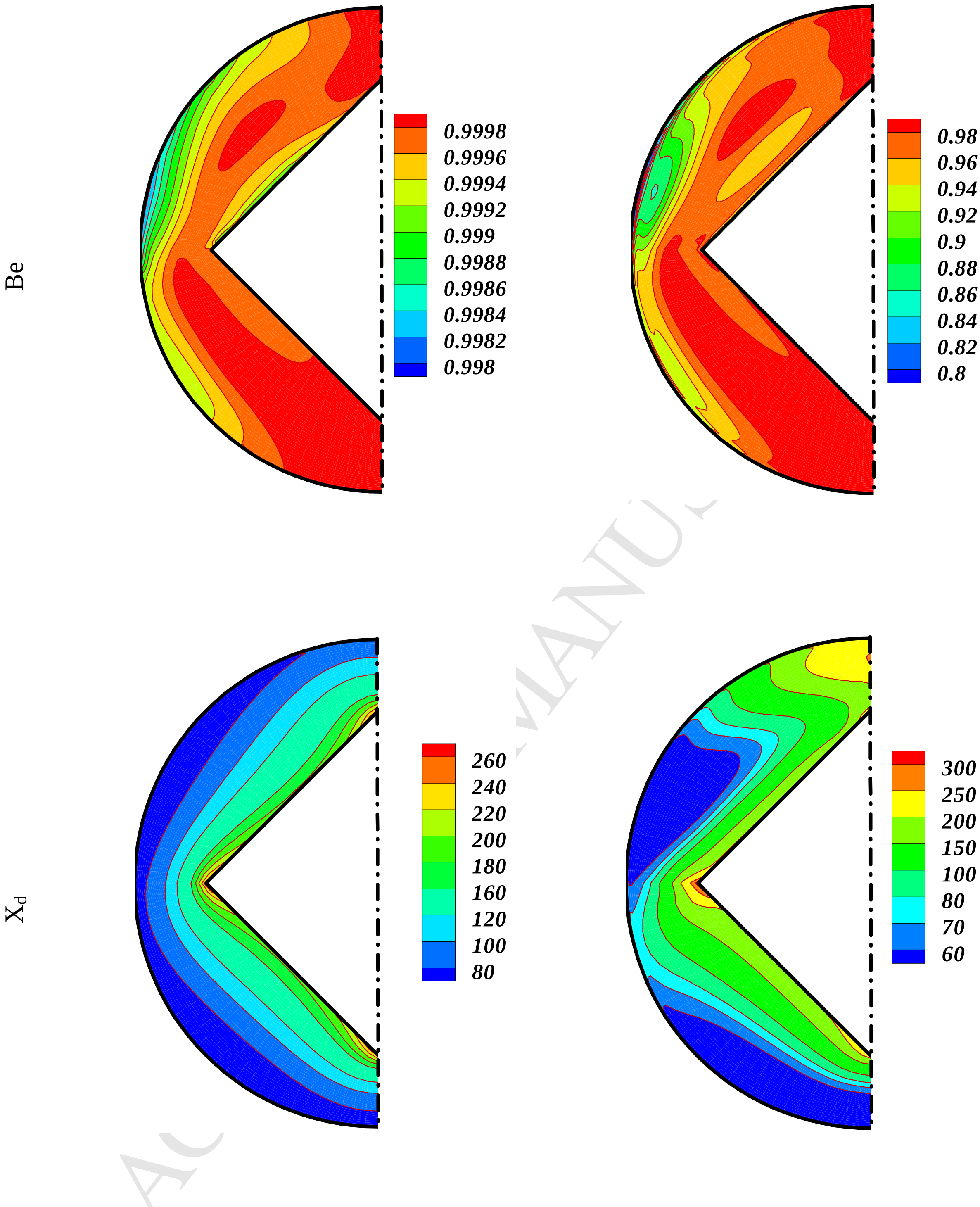

Fig. 4. Exergy and entropy contours for various *Ra* at $\phi = 0.04, Ha = 20, Da = 0.01$

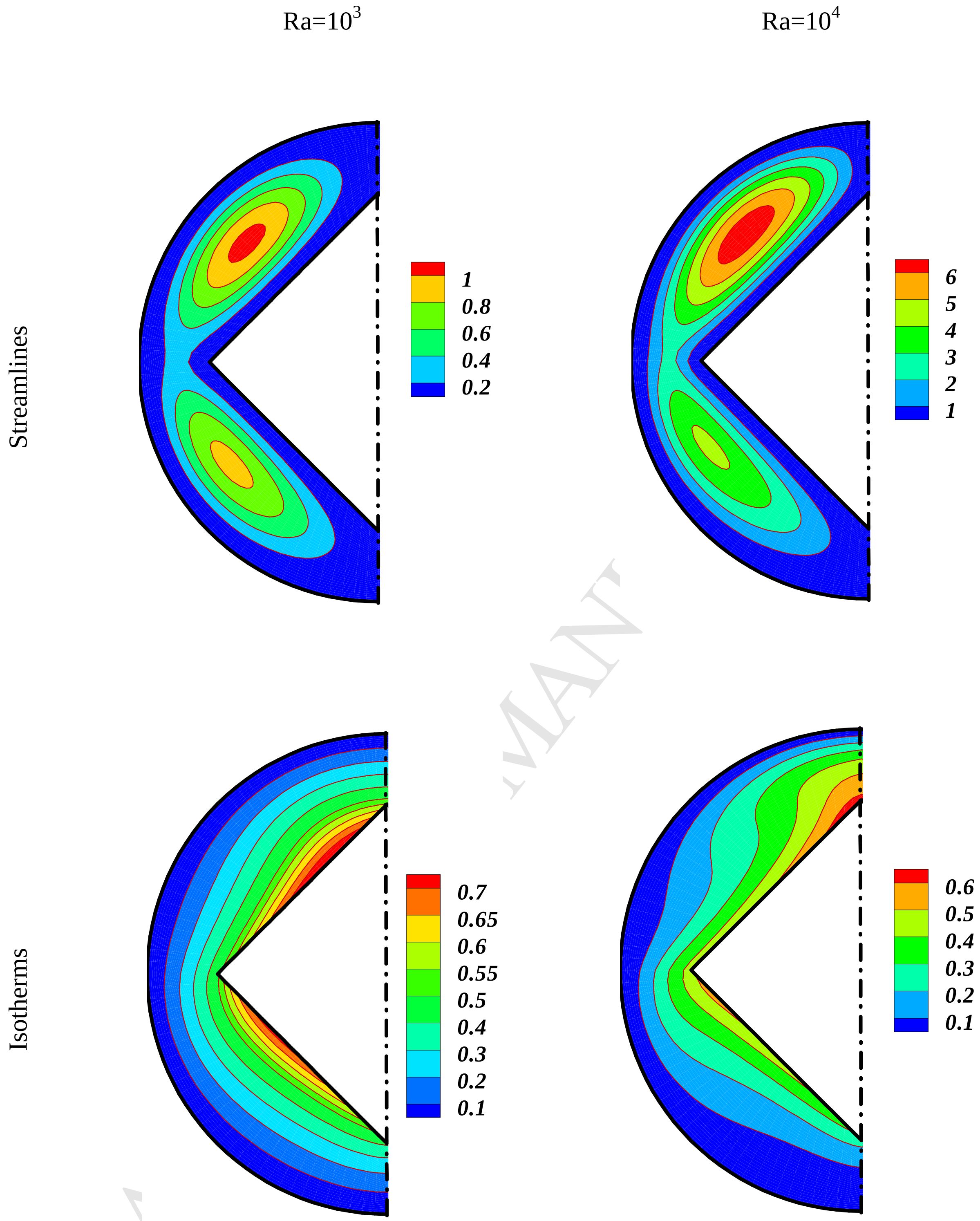
Ra=10^3
Ra=10^4
Streamlines
1
0.8
0.6
0.4
0.2
6
5
4
3
2
1
Isotherms
0.7
0.65
0.6
0.55
0.5
0.4
0.3
0.2
0.1
0.6
0.5
0.4
0.3
0.2
0.1

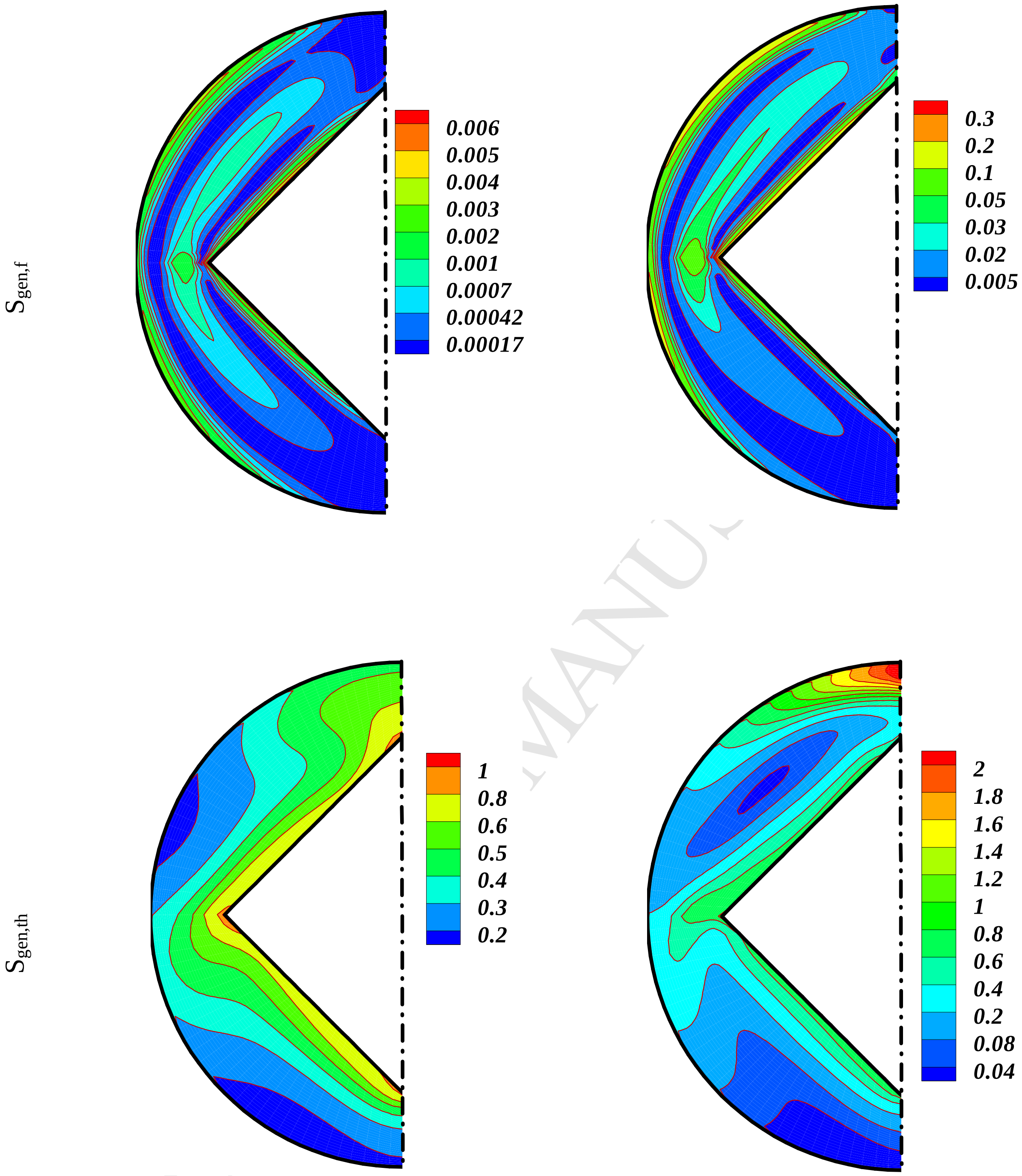

$S_{gen,f}$
0.006
0.005
0.004
0.003
0.002
0.001
0.0007
0.00042
0.00017
0.3
0.2
0.1
0.05
0.03
0.02
0.005
$S_{gen,th}$
1
0.8
0.6
0.5
0.4
0.3
0.2
2
1.8
1.6
1.4
1.2
1
0.8
0.6
0.4
0.2
0.08
0.04

$S_{gen,M}$

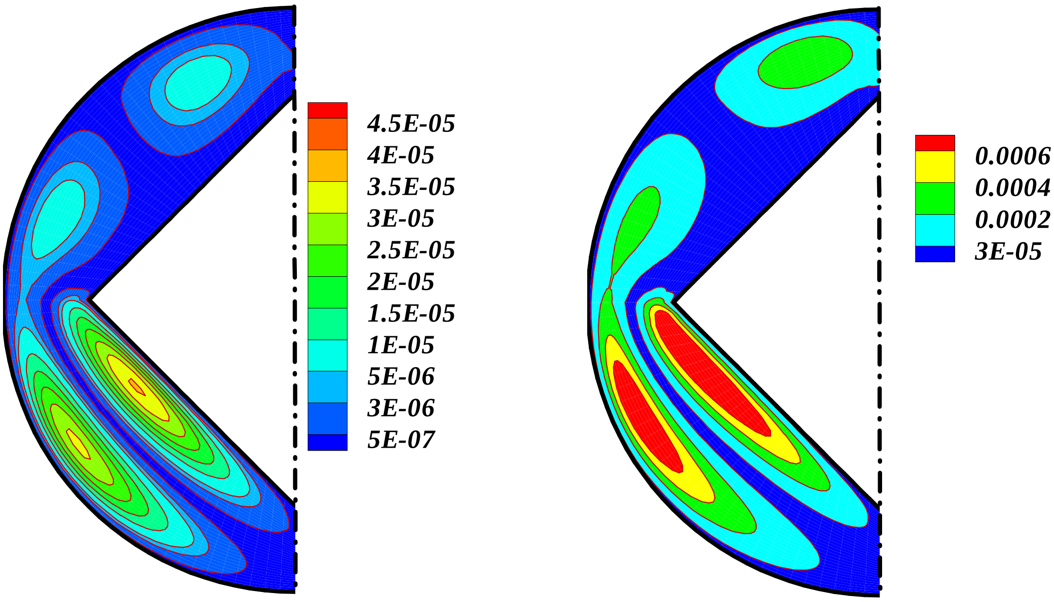
4.5E-05
4E-05
3.5E-05
3E-05
2.5E-05
2E-05
1.5E-05
1E-05
5E-06
3E-06
5E-07
0.0006
0.0004
0.0002
3E-05

$S_{gen,p}$

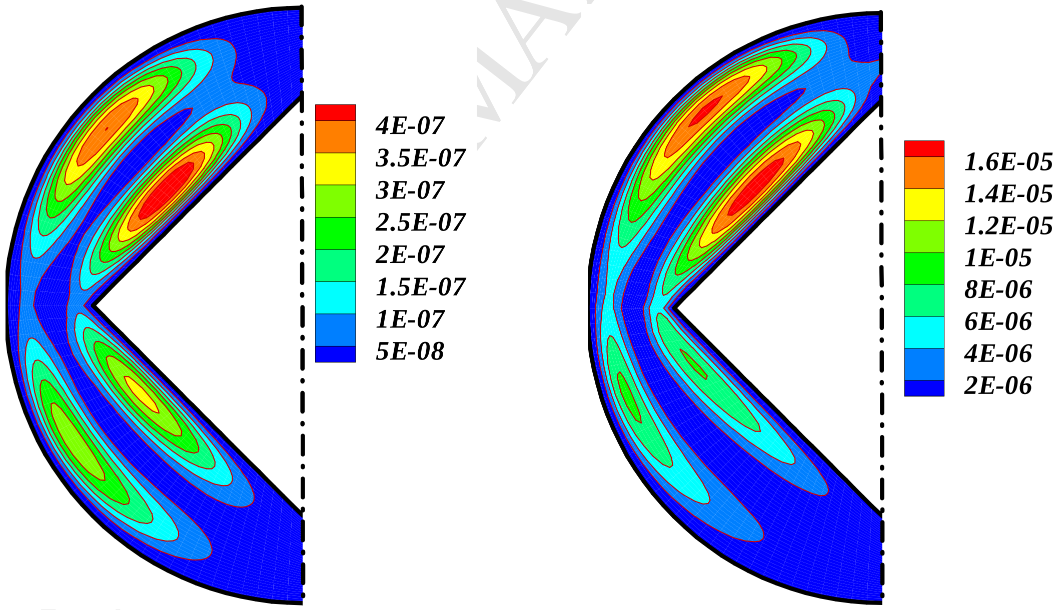
4E-07
3.5E-07
3E-07
2.5E-07
2E-07
1.5E-07
1E-07
5E-08
1.6E-05
1.4E-05
1.2E-05
1E-05
8E-06
6E-06
4E-06
2E-06

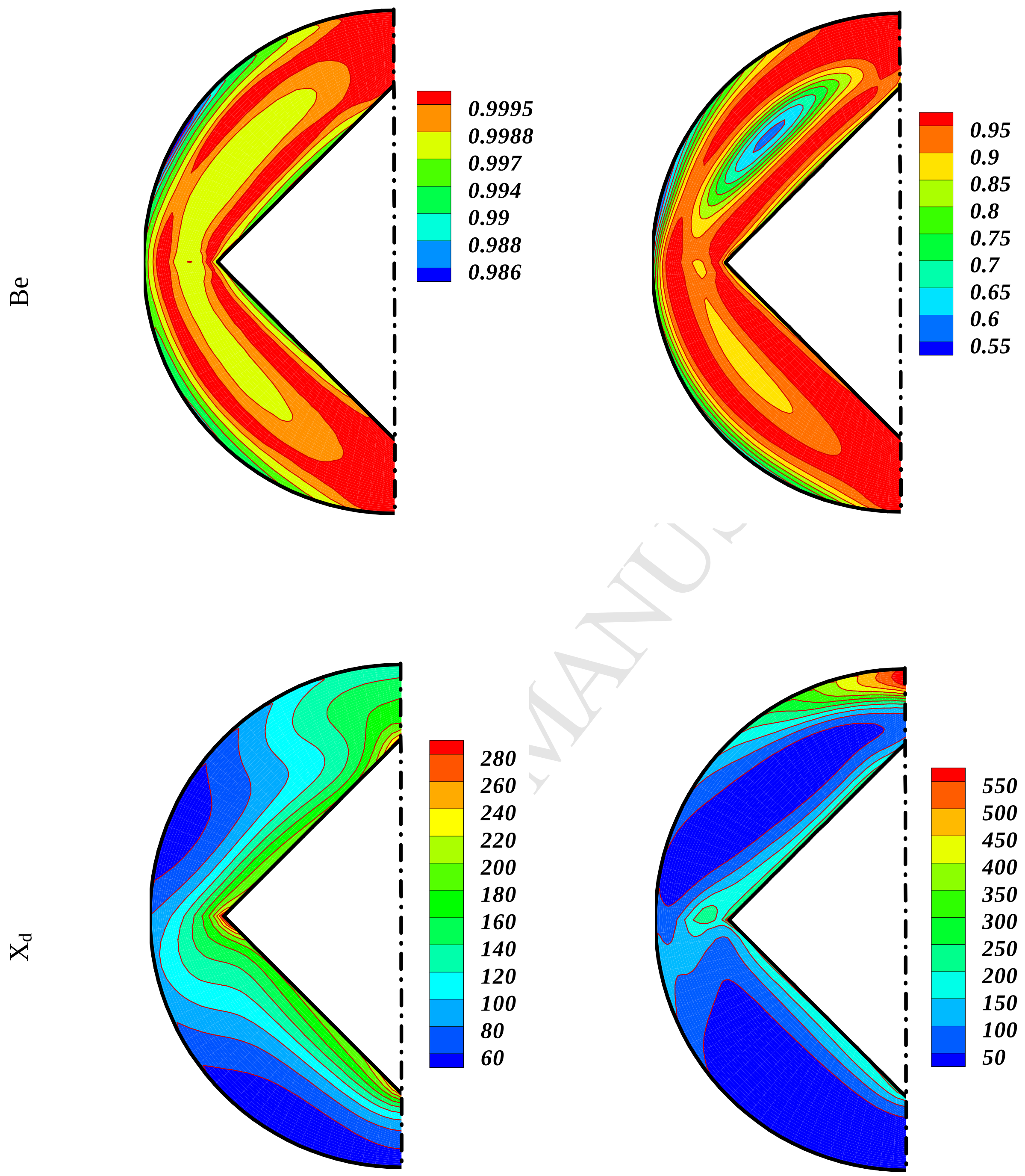

Fig. 5. Exergy and entropy contours for various *Ra* at $\phi = 0.04, Ha = 1, Da = 100$

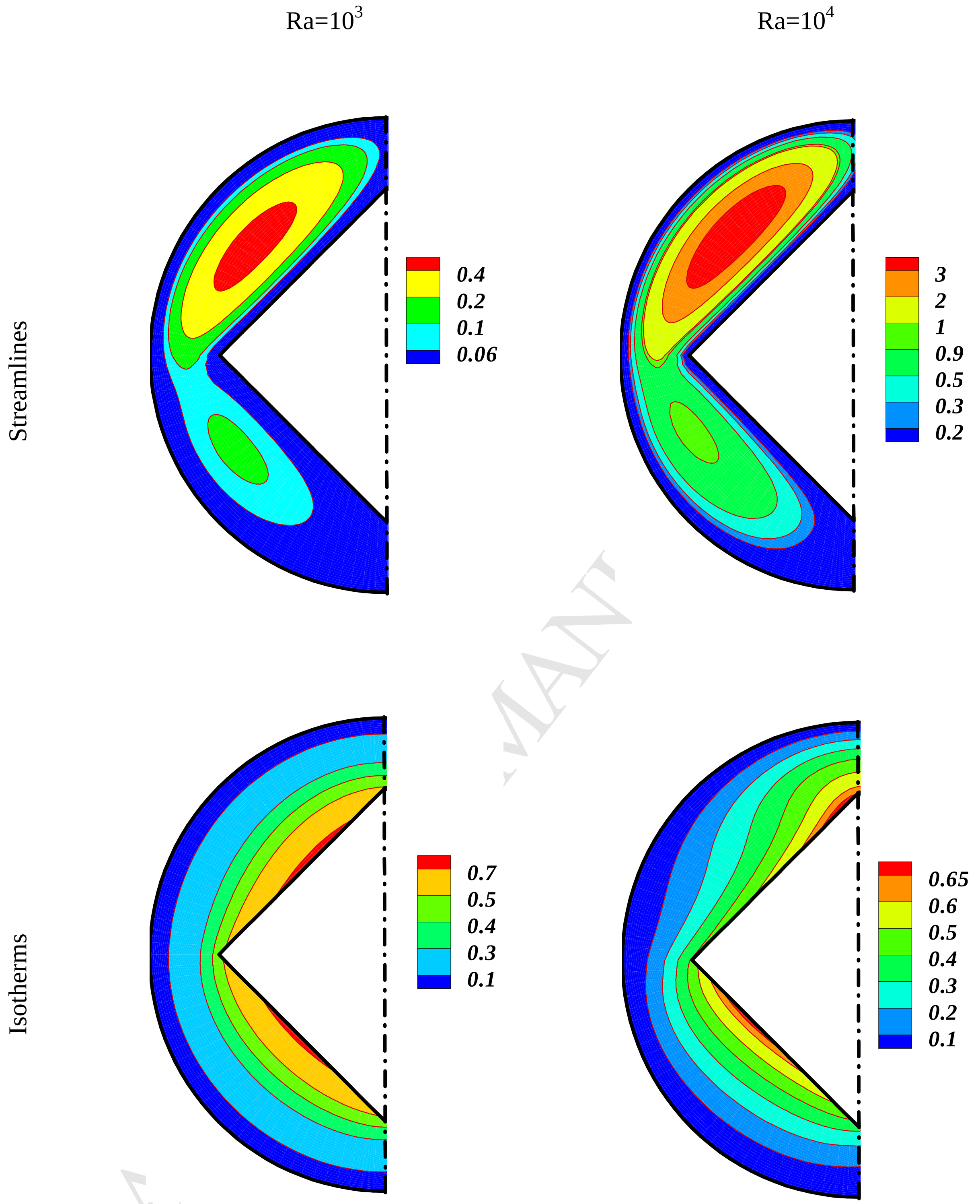

Ra=10^3
Ra=10^4
Streamlines
0.4
0.2
0.1
0.06
3
2
1
0.9
0.5
0.3
0.2
Isotherms
0.7
0.5
0.4
0.3
0.1
0.65
0.6
0.5
0.4
0.3
0.2
0.1

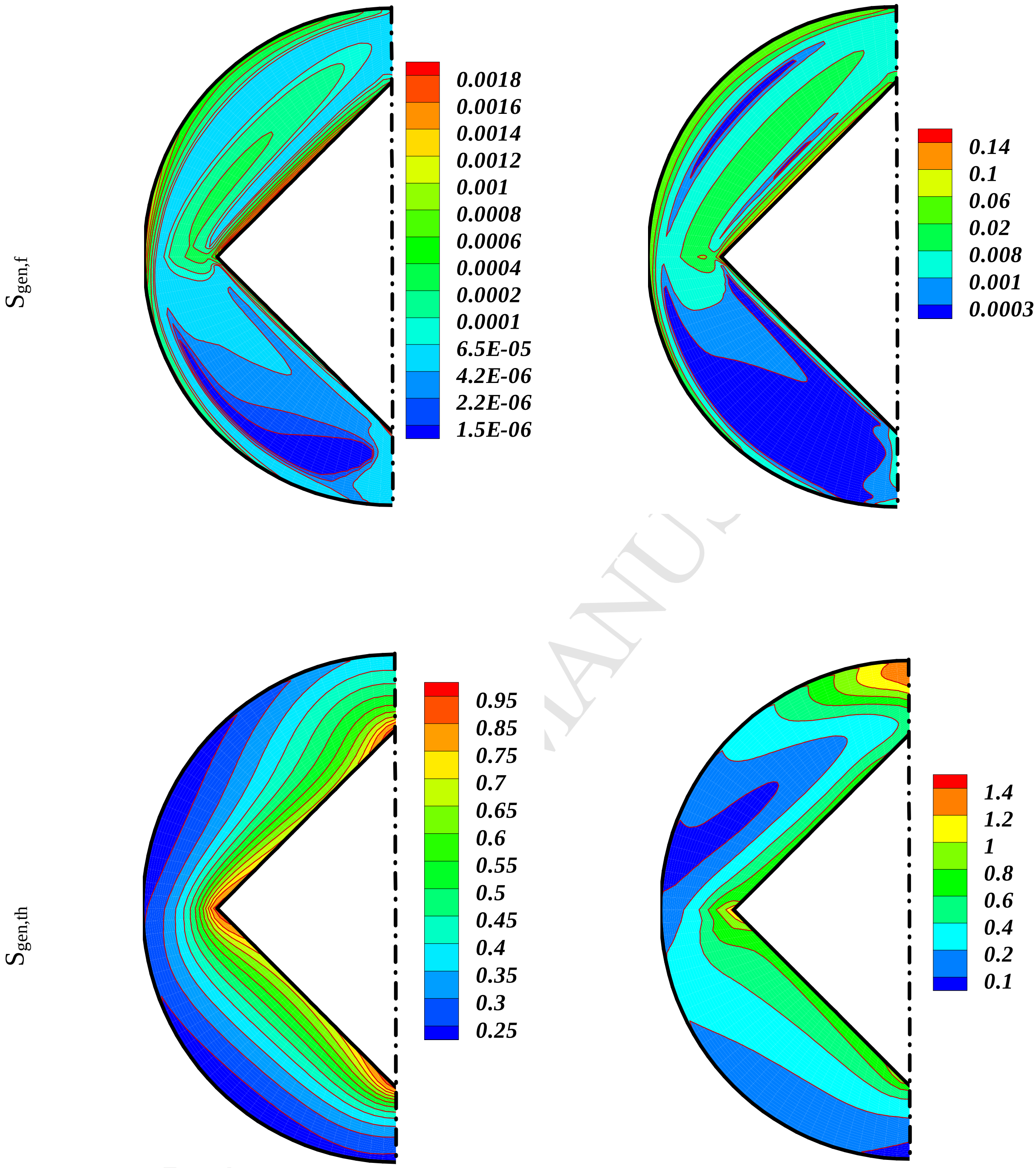

$S_{gen,f}$
0.0018
0.0016
0.0014
0.0012
0.001
0.0008
0.0006
0.0004
0.0002
0.0001
6.5E-05
4.2E-06
2.2E-06
1.5E-06
0.14
0.1
0.06
0.02
0.008
0.001
0.0003
$S_{gen,th}$
0.95
0.85
0.75
0.7
0.65
0.6
0.55
0.5
0.45
0.4
0.35
0.3
0.25
1.4
1.2
1
0.8
0.6
0.4
0.2
0.1

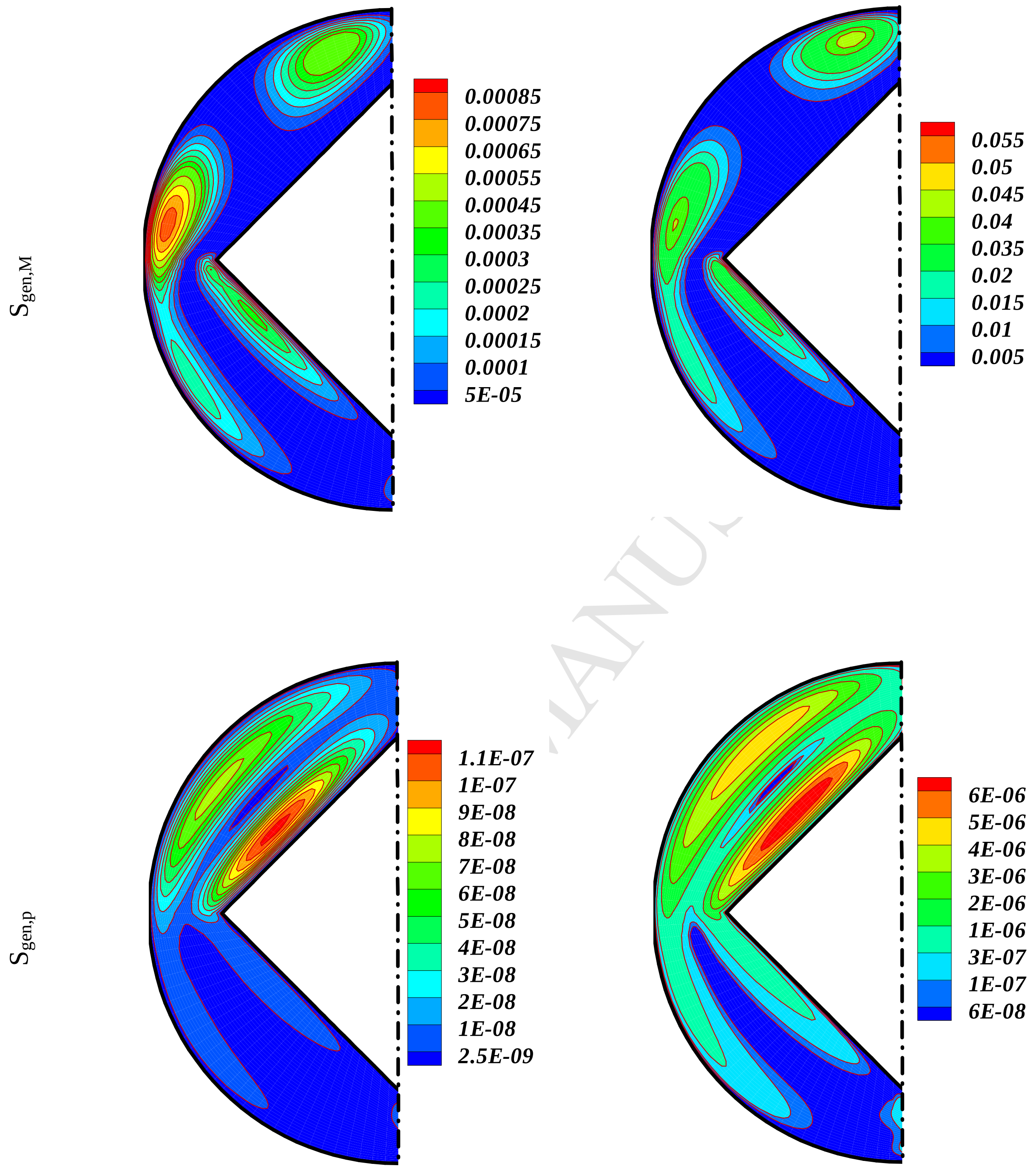

$S_{gen,M}$
0.00085
0.00075
0.00065
0.00055
0.00045
0.00035
0.0003
0.00025
0.0002
0.00015
0.0001
5E-05
0.055
0.05
0.045
0.04
0.035
0.02
0.015
0.01
0.005
$S_{gen,p}$
1.1E-07
1E-07
9E-08
8E-08
7E-08
6E-08
5E-08
4E-08
3E-08
2E-08
1E-08
2.5E-09
6E-06
5E-06
4E-06
3E-06
2E-06
1E-06
3E-07
1E-07
6E-08

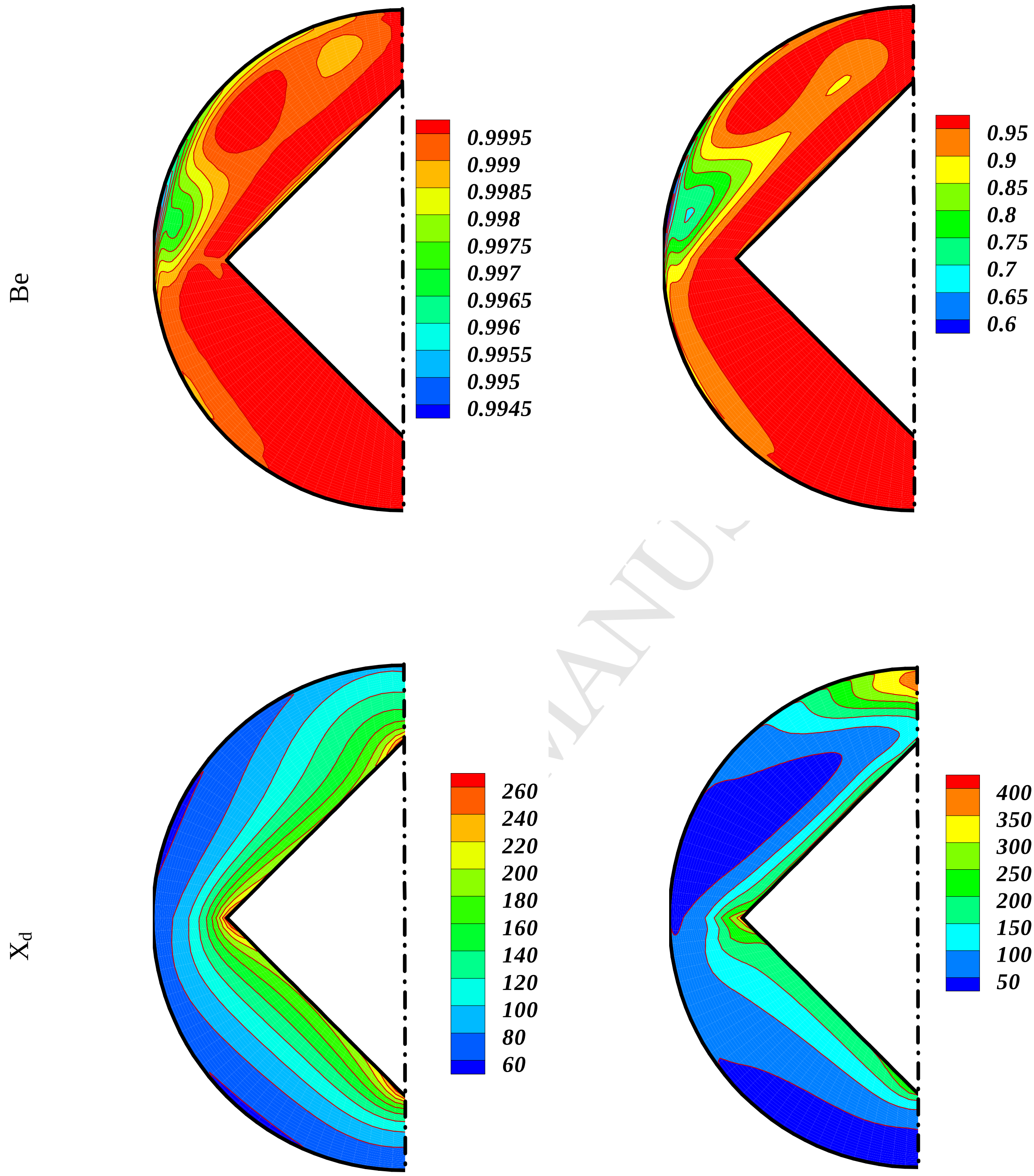

Fig. 6. Exergy and entropy contours for various *Ra* at $\phi = 0.04, Ha = 20, Da = 100$

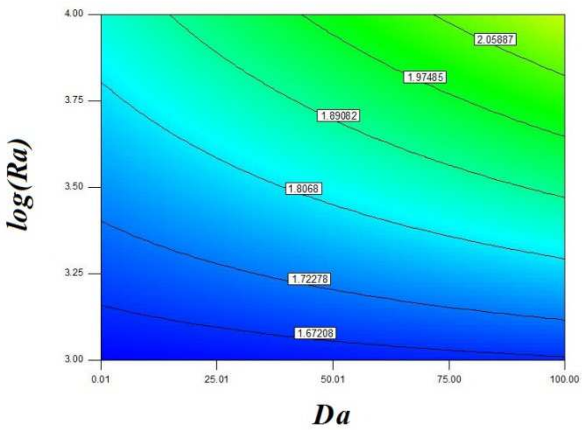

$Ha = 5$

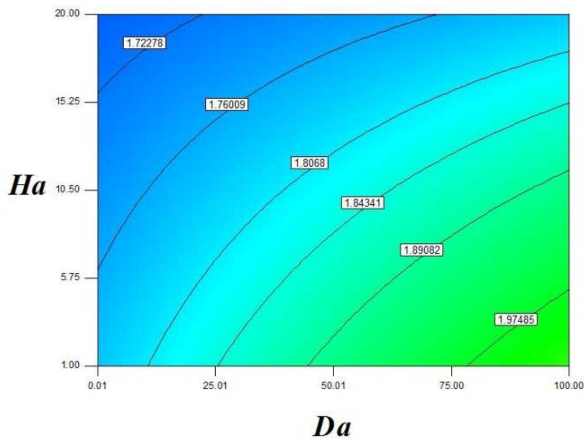

$\log(Ra) = 3.5$

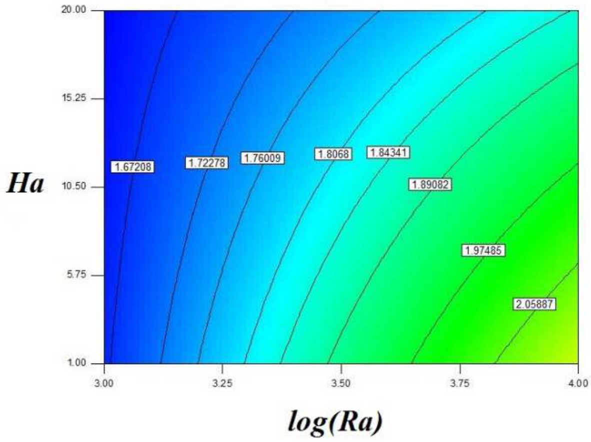

$Da = 50$

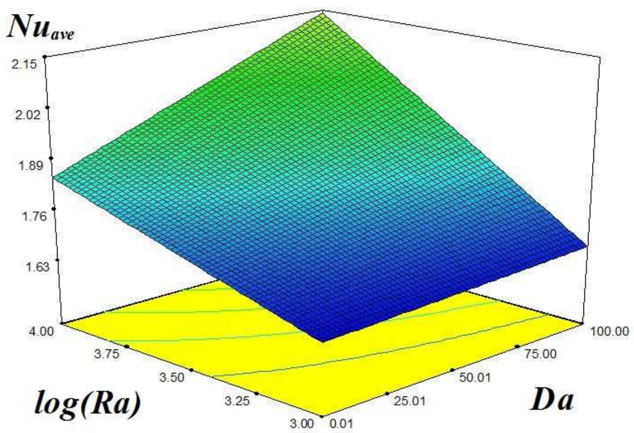

$Ha = 5$

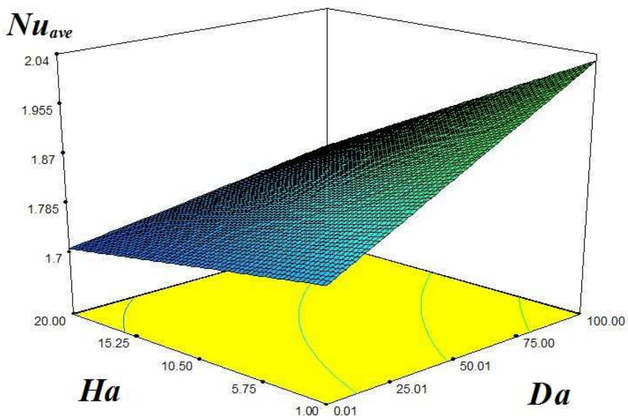

$\log(Ra) = 3.5$

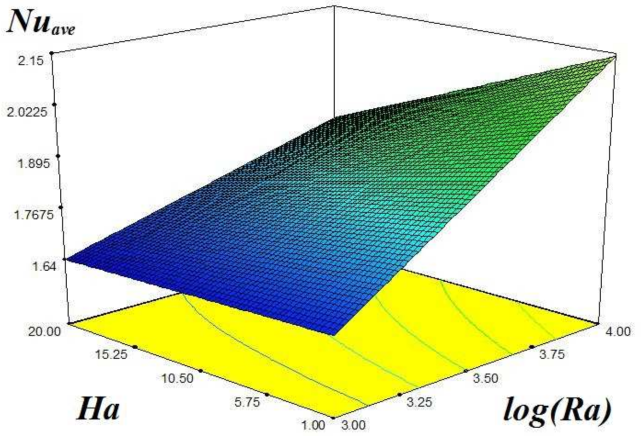

$Da = 50$

Fig. 7. Variation of Nu_{ave} due to change of permeability, buoyancy and Lorentz forces at $\phi = 0.04$.

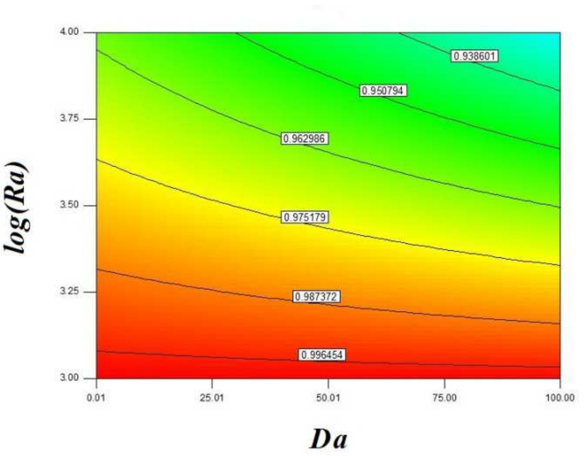

$Ha = 5$

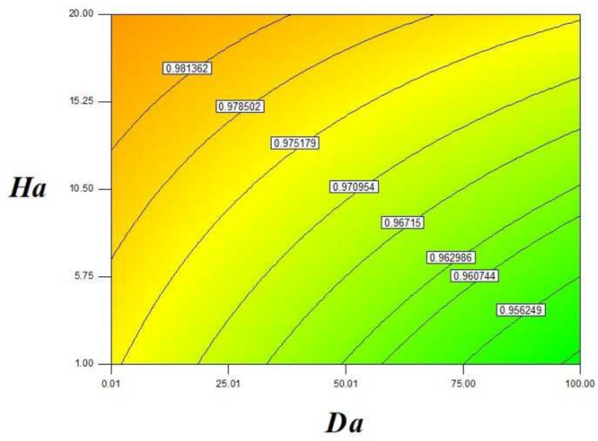

$\log(Ra) = 3.5$

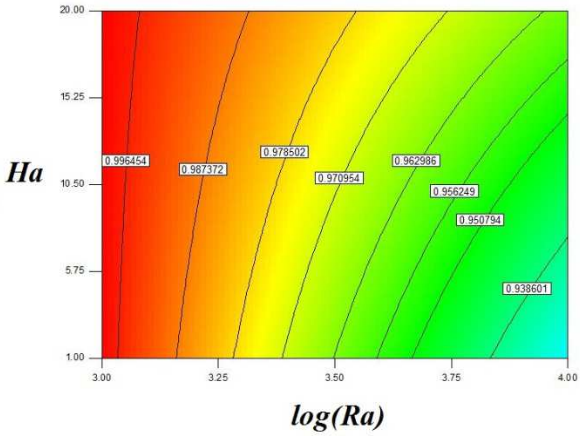

$Da = 50$

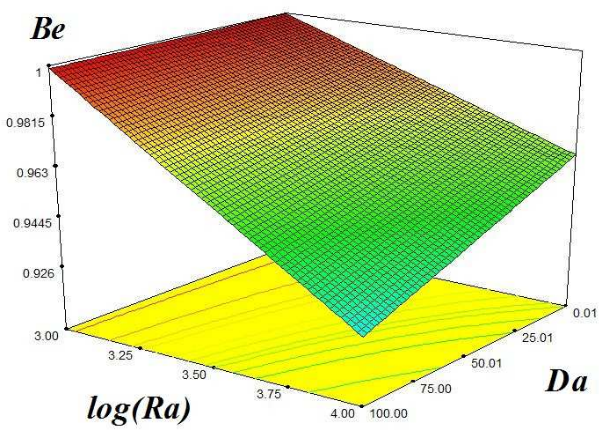

$Ha = 5$

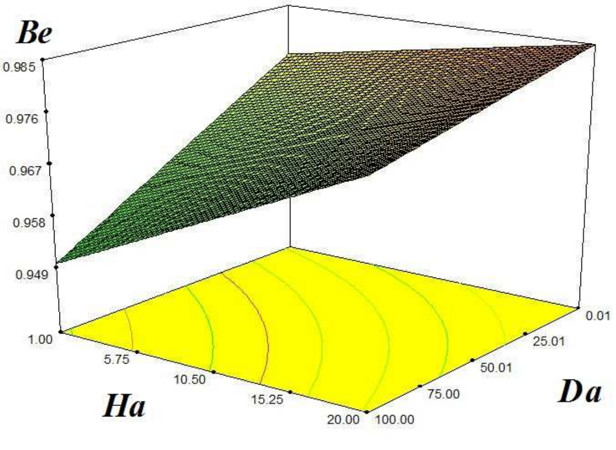

$\log(Ra) = 3.5$

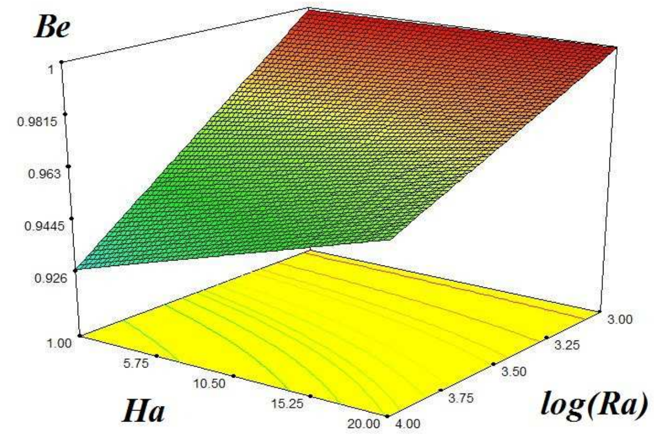

$Da = 50$

Fig. 8. Variation of Be due to change of permeability, buoyancy and Lorentz forces at $\phi = 0.04$.

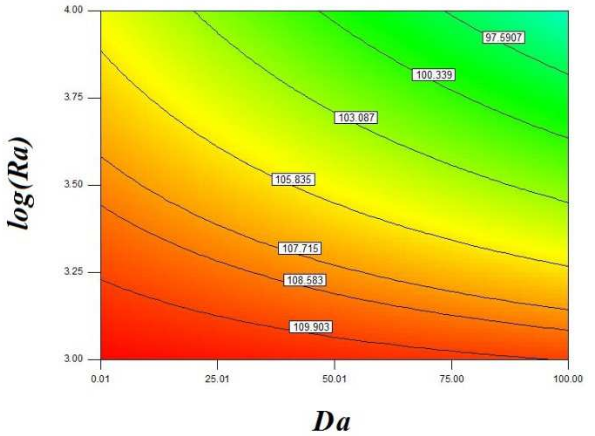

$Ha = 5$

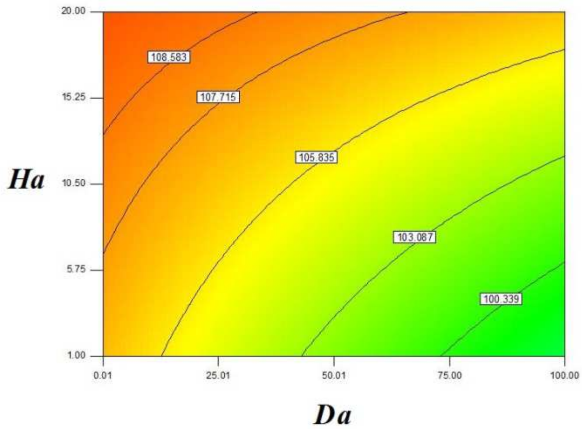

$\log(Ra) = 3.5$

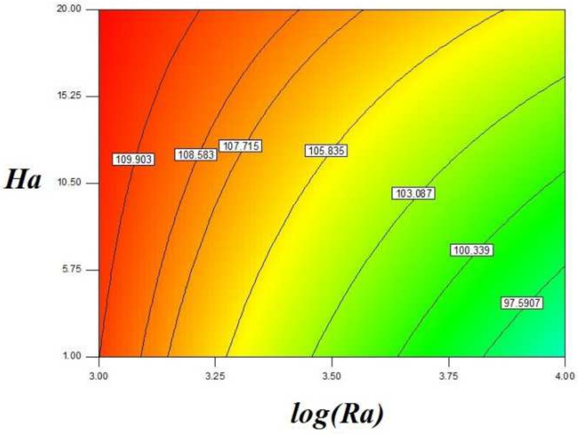

$Da = 50$

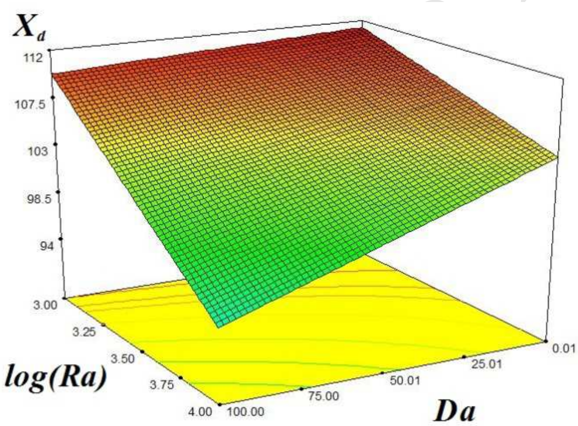

$Ha = 5$

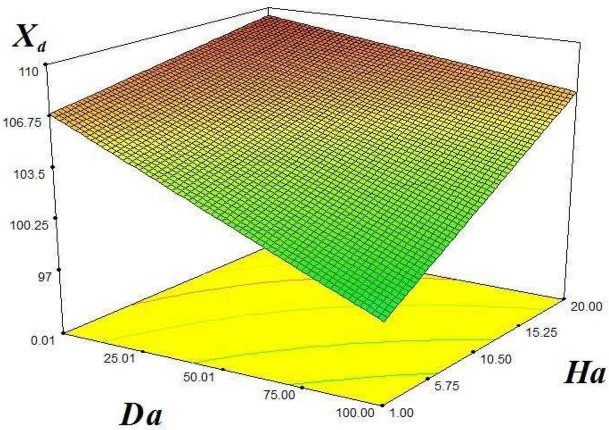

$\log(Ra) = 3.5$

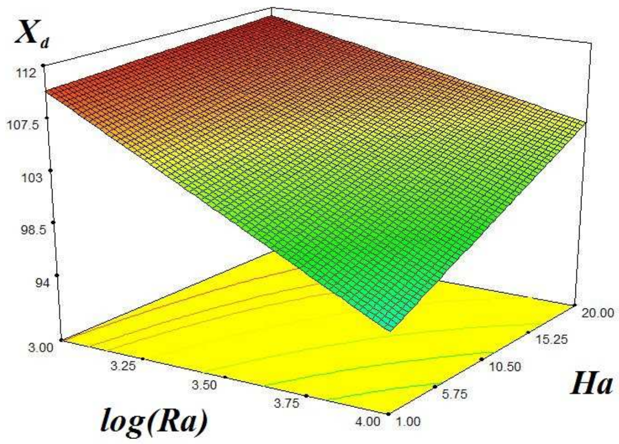

$Da = 50$

Fig. 9. Variation of X_d due to change of permeability, buoyancy and Lorentz forces at $\phi = 0.04$.

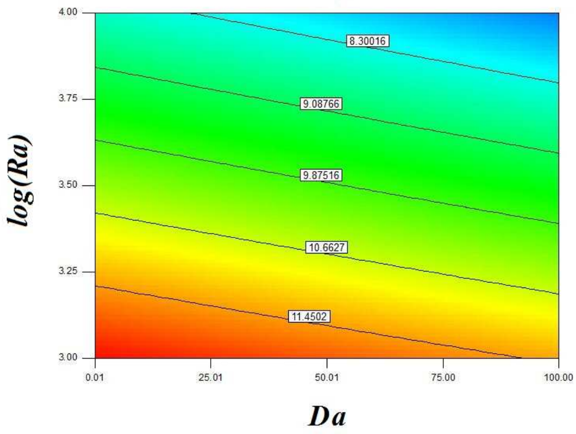

$Ha = 5$

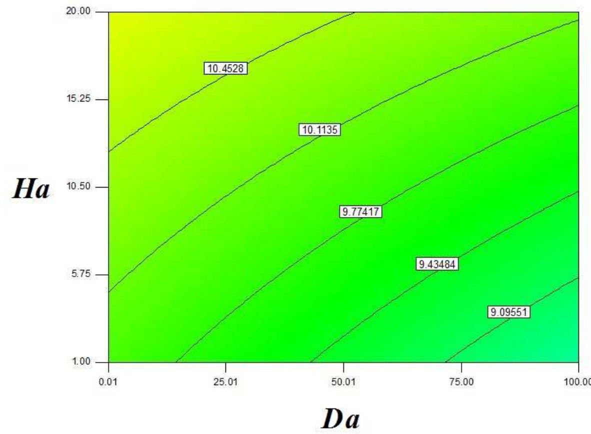

$\log(Ra) = 3.5$

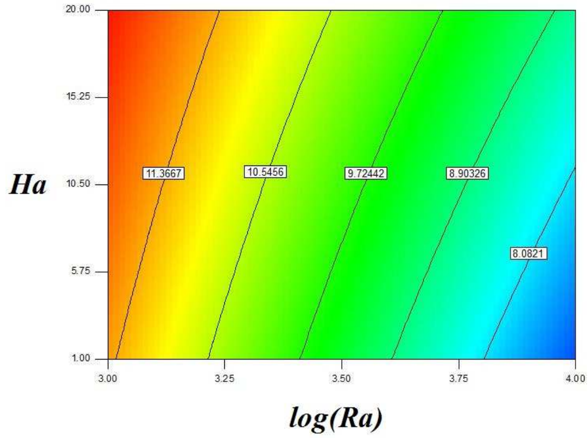

$Da = 50$

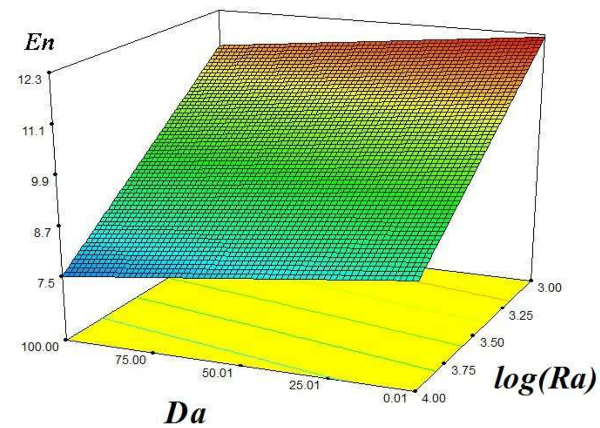

$Ha = 5$

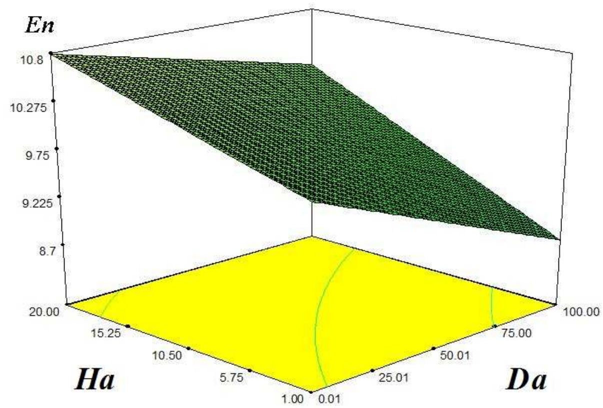

$\log(Ra) = 3.5$

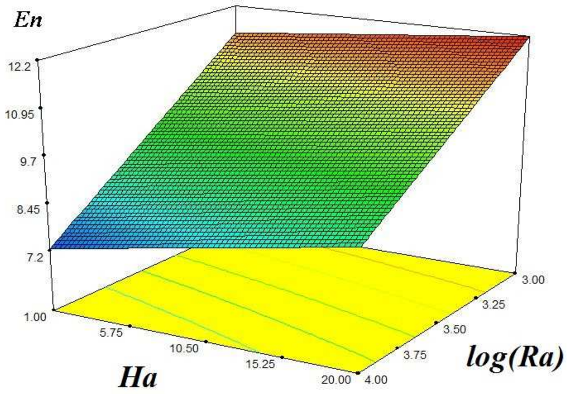

$Da = 50$

Fig. 10. Variation of En due to change of permeability, buoyancy and Lorentz forces at $\phi = 0.04$.

Table1. Properties of H_2O and nanoparticles [30]

Material	$\rho(kg/m^3)$	$\beta\times10^5(K^{-1})$	$\sigma(\Omega\cdot m)^{-1}$	$C_p(j/kgk)$	$k(W/m.k)$
Pure water	997.1	21	0.05	4179	0.613
Fe_3O_4	5200	1.3	25000	670	6

Table2. Various meshes' presentation at $Ra=10^4$, $Ha=20$, $Da=100$ and $\phi=0.04$.

Mesh size in radial direction×angular direction				
51×151	61×181	71×211	81×241	91×271
1.91505	1.91671	1.91772	1.91781	1.91796

Table3. Validation for MHD flow when Pr=0.733 and $Gr=2\times10^4$.

	Ha =10	Ha=50
Present	2.26626	1.09954
Rudraiah et al. (1995)	2.2234	1.0856